Report Documentation Page

Form Approved
OMB No. 0704-0188

1. REPORT DATE	2. REPORT TYPE	3. DATES COVERED
01 DEC 2014	**N/A**	**-**

4. TITLE AND SUBTITLE	5a. CONTRACT NUMBER
Novel osteoinductive photo-cross-linkable chitosan-lactide-fibrinogen hydrogels enhance bone regeneration in critical size segmental bone defects.	5b. GRANT NUMBER
	5c. PROGRAM ELEMENT NUMBER
6. AUTHOR(S)	5d. PROJECT NUMBER
Kim S., Bedigrew K., Guda T., Maloney W. J., Park S., Wenke J. C., Yang Y. P.,	5e. TASK NUMBER
	5f. WORK UNIT NUMBER
7. PERFORMING ORGANIZATION NAME(S) AND ADDRESS(ES)	8. PERFORMING ORGANIZATION REPORT NUMBER
US Army Institute of Surgical Research, JBSA Fort Sam Houston, Texas	
9. SPONSORING/MONITORING AGENCY NAME(S) AND ADDRESS(ES)	10. SPONSOR/MONITOR'S ACRONYM(S)
	11. SPONSOR/MONITOR'S REPORT NUMBER(S)

12. DISTRIBUTION/AVAILABILITY STATEMENT

Approved for public release, distribution unlimited

13. SUPPLEMENTARY NOTES

14. ABSTRACT

15. SUBJECT TERMS

16. SECURITY CLASSIFICATION OF:			17. LIMITATION OF ABSTRACT	18. NUMBER OF PAGES	19a. NAME OF RESPONSIBLE PERSON
a. REPORT	b. ABSTRACT	c. THIS PAGE			
unclassified	**unclassified**	**unclassified**	**UU**	**55**	

Novel osteoinductive photo-cross-linkable chitosan-lactide-fibrinogen hydrogels enhance bone regeneration in critical size segmental bone defects

Sungwoo Kim[1], Katherine Bedigrew[2], Teja Guda[3], William J. Maloney[1], Sangwon Park,[4] Joseph C. Wenke[2], Yunzhi Peter Yang[1,5]

[1]Department of Orthopedic Surgery, Stanford University, Stanford, CA

[2]Extremity Trauma & Regenerative Medicine Task Area, US Army Institute of Surgical Research, San Antonio, TX

[3]Department of Craniomaxillofacial Regenerative Medicine, Dental and Trauma Research Detachment, United States Army Institute of Surgical Research, Fort Sam Houston, TX

[4]Department of Prosthodontics, Dental Science Research Institute and BK21 Project, School of Dentistry, Chonnam National University, Gwangju, Republic of Korea

[5]Department of Materials Science and Engineering, Stanford University, Stanford, CA

* Corresponding author:

Yunzhi Peter Yang, Ph.D.
Associate Professor
Department of Orthopedic Surgery
Stanford University
300 Pasteur Drive
Edwards R105
Stanford, CA 94305
Tel: 650-723-0772
Fax: 650-724-5401
Email: ypyang@stanford.edu

Abstract

The purpose of this study was to develop and characterize a novel photo-cross-linkable chitosan-lactide-fibrinogen (CLF) hydrogel and evaluate the efficacy of bone morphogenetic protein-2 (BMP-2) containing CLF hydrogel for osteogenesis *in vitro* and *in vivo*. We synthesized the CLF hydrogels and characterized their chemical structure, degradation rate, compressive modulus, and *in vitro* BMP-2 release kinetics. We evaluated bioactivities of the BMP-2 containing CLF hydrogels (0, 50, 100, and 500 ng/ml) *in vitro* using W-20-17 preosteoblast mouse bone marrow stromal cells and C2C12 mouse myoblast cells. The effect of BMP-2 containing CLF gels (0, 0.5, 1, 2, and 5μg) on bone formation was evaluated using rat critical size segmental bone defects for 4 weeks. FTIR spectra and SEM images showed chemical and structural changes by addition of fibrinogen into chitosan-lactide copolymer. Incorporation of fibrinogen molecules significantly increased compressive modulus of the hydrogels. *In vitro* BMP-2 release study showed initial burst releases from the CLF hydrogels followed by sustained releases, regardless of the concentration of the BMP-2 over 4 weeks. Cells in all groups were viable in the presence of the hydrogels regardless of BMP-2 doses, indicating non-cytotoxicity of hydrogels. Alkaline phosphate activity and mineralization of cells exhibited dose dependence on BMP-2 containing CLF hydrogels. Radiographs, microcomputed tomography, and histology confirmed that the BMP-2 containing CLF hydrogels prompted neo-osteogenesis and accelerated healing of the defects in a dose-dependent manner. Thus the CLF hydrogel is a promising delivery system of growth factors for bone regeneration.

Keywords: Chitosan; Lactide; Fibrinogen; Photo-cross-linkable hydrogel; BMP-2; Osteoblastic differentiation; W-20-17; C2C12; Critically sized bone defect, New bone formation

1. Introduction

Bone morphogenetic protein-2 (BMP-2) is a potent osteoinductive factor and plays an important role in bone regeneration by stimulating endochondral ossification via chemotaxis, migration, proliferation and osteogenic differentiation of mesenchymal stem cells [1-4]. However, BMP-2 administered in the form of a buffer solution has a short biological half-life, rapid clearance, potential harmful side effects, and is very costly in systematic delivery [2, 5-6]. Improved efficacy of BMP-2 induced bone formation can be achieved by using biodegradable delivery systems to overcome the limitations aforementioned [2, 7]. BMP-2 in combination with an absorbable collagen sponge (ACS) is the FDA-approved device for clinical applications including lumbar spine fusion, open tibial fractures, and sinus augmentation [4, 7-9]. However, the concerns about side effects associated with a rapid burst release and the risk of immunogenic responses have necessitated new delivery strategies that enable a controlled and sustained release of BMP-2 at the physiologically relevant dose to enhance therapeutic outcome [10-14]. The ideal delivery system should maintain the structural integrity of the defects, spatially and temporally present bioactivity to guide surrounding cells, and gradually degrade corresponding to the rate of tissue regeneration [15-16].

In this regard, hydrogels have been broadly studied for delivery of growth factors to facilitate tissue integration and regeneration, as well as restoring the function of a damaged tissue [13-16]. Recent studies have demonstrated that introduction of growth factor binding ligands to polymer-based delivery systems can maintain bioactivities of the growth factors over extended periods of time and allow cell-mediated proteolysis to transiently release the bound growth factors [12, 16-17]. The growth factor binding ligands enhance the strength of interactions between growth factors and the materials, leading to improved tissue regeneration [15-17]. The choice of growth factor binding protein depends on its affinity to specific growth factor in the specific target of interest. For example, BMP-2 binds to the components of the extracellular matrix (ECM) by interaction with heparan-sulfate proteoglycans [12, 18]. The basic N-terminal

domains of BMP-2, including arginine, lysine, and histidines, are key components of the heparin-binding sites [18-20]. Therefore, the heparin-binding affinity can be used to enhance controlled release of BMP-2 in response to cell-mediated enzymatic activity during bone healing [17-23].

Herein, we present a photo-cross-linkable chitosan-lactide-fibrinogen (CLF) hydrogel as a carrier for delivery of BMP-2 and evaluated the delivery efficacy of BMP-2 containing CLF hydrogels on osteogenesis *in vitro* and *in vivo*. This CLF hydrogel was developed based on our previous work on a chitosan-lactide (CL) hydrogel by addition of fibrinogen [24]. Fibrinogen contains a heparin-binding domain, which was used to improve BMP-2 binding affinity [21, 25]. Fibrinogen has been extensively studied for human use in a number of clinical applications such as a tissue sealant, growth factor delivery, and a tissue engineered scaffold [21-22, 26]. Fibrinogen has proteolytically degradable sites and adhesive ligands for cell surface integrins [10, 17, 26]. Our CLF hydrogel was designated to contain tunable mechanical properties, hydrolytically degradable amide and ester linkages, and excellent protein binding affinities. The cross-linked hydrogel networks are formed by a radical polymerization upon application of ultra-violet (UV) light. The properties of the CLF hydrogels, such as swellability, stiffness, and degradability, can be readily adjusted by changing ratios of chitosan to lactide and cross-linking density via UV exposure time. In this regard, we have optimized the CLF hydrogels for sustained delivery of BMP-2 over several weeks to promote new bone formation.

In this study, we first synthesized the photo-cross-linkable CLF hydrogels and characterized their chemical structure, compressive modulus, degradation rate, and *in vitro* BMP-2 release kinetics. Then, we examined bioactivities of the CLF hydrogel mediated BMP-2 using W-20-17 preosteoblast mouse bone marrow stromal cells and C2C12 mouse myoblast cells *in vitro*. The delivery efficacy of BMP-2 was evaluated by measuring cytotoxicity, alkaline phosphatase (ALP) activity, and mineralization according to different doses (0, 50, 100, or 500 ng/ml). In addition, we investigated the new bone formation in a critically sized rat femoral defect by implanting the CLF hydrogels loaded with BMP-2 (0, 0.5, 1, 2, and 5μg) for 4 weeks. This

study has demonstrated that the photo-cross-linkable CLF hydrogel can effectively deliver BMP-2 to regulate cell response and enhance osteogenesis both *in vitro* and *in vivo*.

2. Materials and Methods

2.1. Materials

Chitosan (≥ 310 kDa, 75% or greater degree of deacetylation) and methacrylic anhydride were purchased from Sigma-Aldrich (St Louis, MO). D,L-Lactide was purchased from Ortec (Piedmont, SC). Human fibrinogen was obtained from Enzyme Research Labs (South Bend, IN). Human bone morphogenetic protein-2 (BMP-2) was obtained from Medtronic (Minneapolis, MN). All other chemicals were reagent grade and were used as received. UV light source (Omnicure S2000) was purchased from Lumen Dynamics Group Inc (Ontario, Canada).

2.2. Synthesis of CLF hydrogels

A 1 % (w/v) chitosan solution was prepared by stirring powdered chitosan in 0.75% (v/v) aqueous acetic acid at room temperature overnight. The insoluble particles in the chitosan solution were removed by filtration. An aqueous solution of lactic acid was prepared by dissolving powdered D,L-Lactide in DMSO (dimethyl sulfoxide) at 80°C. The mass ratio of chitosan to lactide was 8:1. The mixture of chitosan and lactide was stirred using a magnet stirrer for 1 hour at 80 °C. Tin (II) 2-ethylhexanoate and triethylamine (TEA) were added dropwise. The mixture was reacted at 80 °C with magnetic stirring for 20 hours in nitrogen atmosphere. The mixture was dialyzed in distilled water using dialysis tubing (molecular weight cut off: 14,000) for 1day. 2.5 % (w/v) methacrylic anhydride was added into the dialyzed mixture dropwise, and the reaction was continued for 8 hours at 60 °C. The mixture was dialyzed in distilled water using dialysis tubing (molecular weight cut off: 14,000) for 7 days. The obtained solution was then freeze-dried for 2-3 days and stored at -20°C until use. For the CLF hydrogel formulation, the freeze-dried samples were reconstituted as a 2.5 % (w/v) in distilled water. The prepolymer

solution was mixed with fibrinogen (3.6 mg/ml) at 4 °C overnight. The photoinitiator (Irgacure 2959, CIBA Chemicals) was dissolved completely into distilled water at 70°C. The photoinitiator solution was sterile-filtered through a 0.22 μm filter and then added to the prepolymer solutions to make a final concentration of 0.5 % (w/v). The prepolymer solutions were then exposed to 6.9 mW/cm^2 UV light to allow for free radical polymerization by photo-cross-linking.

2.3. Characterization of CLF hydrogels

2.3.1. Fourier transform infrared spectroscopy (FTIR) spectra

In order to investigate chemical structure of prepolymer solutions, including CL and CLF, FTIR spectra were obtained using a Bruker Vertex 70 FTIR spectrometer coupled to a PC with analysis software. Samples were placed in the holder directly in the IR laser beam. All spectra were recorded by transmittance mode (40 times scanning, 800-4000 cm^{-1}).

2.3.2. Scanning electron microscopy (SEM)

The internal microstructures of the CL and CLF hydrogels were investigated by SEM. The effect of fibrinogen on the morphological change of the CL hydrogels was observed. The hydrogel samples were incubated into PBS (pH 7.4) at 37°C for 1 day and lyophilized overnight (Freezone, LABCONCO). The samples were sputter-coated with gold and examined under a scanning electron microscope (Hitachi S-3400N VP SEM) operated at 10 kV voltages.

2.3.3. Mechanical testing

Unconfined compression tests were performed to determine the mechanical properties of the CL and CLF hydrogels using an Instron 5944 materials testing system (Instron Corporation, Norwood, MA) fitted with a 10 N load cell (Interface Inc., Scottsdale, Az). The prepolymer solution was pipetted into a cylindrical Teflon mold and exposed to 6.9 mW/cm^2 UV light for 200s. The diameter (~6 mm) and thickness (~3 mm) of the samples were measured using digital

calipers and the material testing system's position read-out, respectively. Before each test, a preload of approximately 2 mN was applied. The upper platen was then lowered at a rate of 1% strain/sec to a maximum strain of 30%. Load and displacement data were recorded at 100 Hz. The compressive modulus was determined for strain ranges of 10-20% from linear curve fits of the stress-strain curve. All tests were conducted in PBS solution at room temperature.

2.3.4. *In vitro* degradation characteristics

In vitro degradation behavior of the hydrogels was investigated by comparing CL hydrogels with CLF according to different pHs and enzymatic activities. The swelling behavior or degradation profile of the hydrogels was determined by measuring the wet remaining ratio of the hydrogels in phosphate-buffered saline (PBS) solution. The hydrogels were surface dried and weighed (W_0). Then the hydrogels were placed into PBS (pH 7.4), PBS (pH 4), or 1mg/ml collagenase A containing PBS (pH 7.4) at 37°C. At designated time points over a period of 4 weeks, the samples were taken out and weighed again (W_1). The wet weight remaining ratio was calculated as follow: Wet weight remaining ratio (%) = $W_1 / W_0 \times 100\%$

2.4. *In vitro* BMP-2 release study

To study the release kinetics of BMP-2 from the CLF hydrogels, two different concentrations of BMP-2 were directly loaded into the CLF hydrogels formulation (10 ng/ml and 100 ng/ml). Briefly, BMP-2 was mixed with prepolymer solution to form a homogenous solution, and then they were preserved at 4°C overnight prior to the experiment. The mixture was then pipetted into a cylindrical Teflon mold and exposed to 6.9 mW/cm^2 UV light. The hydrogels with diameter of 6 mm and thickness of 3 mm were prepared. Each sample was placed in a container with 1 ml of PBS (pH 7.4) and incubated at 37°C for 28 days. At designated time points, 150 µl aliquots of the release medium were sampled and the same amount of fresh PBS (pH 7.4) was added into each container. In the collected fractions, the cumulative amount and percentage of

BMP-2 from the CLF hydrogels were determined as a function of time by a BMP-2 ELISA kit (R&D systems, MN). The optical density of each well was determined using a microplate reader at 450 nm with a correction setting of 540 nm (TECAN Infinite F50).

2.5. *In vitro* bioactivities

2.5.1. Cell culture

Two different cell lines, W-20-17 preosteoblast mouse bone marrow stromal cells and C2C12 mouse myoblast cells, were purchased from ATCC (Manassas, VA). They were grown and maintained in DMEM media with 10% FBS, 1% antibiotic/antimycotic mixture, 5ml of L-glutamine (200mM), and sodium pyruvate. The cells were cultured in an incubator supplied with 5% CO_2 at 37°C. The culture medium was changed every 3 days.

2.5.2. Cytotoxicity of hydrogels

The cytotoxicity of the CLF hydrogels was quantitatively examined by an indirect cell culture. The hydrogels were loaded with different concentrations of BMP-2 (0, 50, 100, or 500 ng/ml) as described above and placed into cell culture inserts (BD BioCoat™ Control Cell Culture inserts). Two different cell lines (W-20-17 and C2C12) were used. The cells were seeded at a density of 30,000 cells/well in the bottom of 24-well plates and the hydrogels were placed into the upper chamber with culture medium. After 1 and 3 days of the incubation, the number of viable cells was determined quantitatively using a MTS assay according to the manufacturer's instructions. The light absorbance at 490 nm was recorded using a micro plate reader (TECAN Infinite F50). Before the assay, the cellular morphology was observed qualitatively using a Zeiss Axiovert 200 microscope (Carl Zeiss Microimaging, Thornwood, NY). Photomicrographs of cells were processed using a software (Zeiss, AxioVision).

2.5.3. Dose effects of BMP-2 on alkaline phosphatase (ALP) activities in cells

In order to investigate the effect of different concentrations of BMP-2 on the presence of ALP, the W-20-17 and C2C12 cell lines were cultured in the DMEM media containing the CLF hydrogels. Cells were seeded in the bottom of 24-well plates at a density of 60,000 cells/well. The hydrogels loaded with BMP-2 (0, 50, 100, or 500 ng/ml) were placed into the inserts and added into the 24-well plates. After 7 days of the incubation, the cell layers were washed twice with PBS (pH 7.4) and then lysed with 1 ml of 0.2% Triton X-100 by three freeze-thaw cycles, which consisted of freezing at -80 °C for 30 minutes immediately followed by thawing at 37 °C for 15 minutes. Cell response to BMP-2 released from the hydrogels was determined by ALP activity and by double stranded DNA (dsDNA). In brief, 50 µl aliquots of the cell lysates were sampled and added to 50 µl of working reagent in a 96-well assay plate. The working regent contains equal parts (1:1:1) of 1.5M 2-amino-2-methyl-1-propanol (Sigma), 20 mM p-nitrophenyl phosphate (Sigma), and 1 mM magnesium chloride. The samples then were incubated for 1 hour at 37°C. After incubation, the reaction was stopped with 100 µl of 1N sodium hydroxide on ice. ALP activity was determined from the absorbance using a standard curve prepared from p-nitrophenol stock standard (Sigma). The absorbance was measured at 492 nm using a microplate reader (TECAN Infinite F50). For dsDNA, 50 µl aliquots of the cell lysates were added in a 96-well assay plate. Each 50 µl of a 1:200 dilution of picogreen (Invitrogen) was added to each well and incubated for 5 min in the dark. The assay plate was read at 485 nm excitation and 528 nm emissions using a BioTek FLx800 plate reader. The dsDNA content was calculated using a standard curve made by a provided dsDNA standard sample. The ALP specific activity of cells was then calculated by normalizing to dsDNA. ALP activity was expressed as nmol/ng.

2.5.4. Alizarin Red S staining for calcium mineralization

Calcium mineral content within the cell layers was determined qualitatively and quantitatively by Alizarin Red S staining (AR-S). Cells were seeded in 24-well plates at a density of 30,000 cells/well and incubated in DMEM for 1 day, and then the culture medium was

changed to osteogenic media containing 10% FBS, 10 mM β-glycerophosphate, 10 nM dexamethasone, and 50 mg/ml ascorbic acid. The hydrogels were loaded with different concentrations of BMP-2 (0, 50, 100, or 500 ng/ml). The hydrogels loaded with BMP-2 were placed into the inserts and added into the well plates. At the end of each time point (10 and 21 days of incubation), the cell layers were washed with PBS (pH 7.4) twice and fixed in ice-cold 50 % ethanol at 4 °C for 30 minutes. After washing with distilled water, they were completely dried at room temperature and stained by adding 1 ml of 1% Alizarin Red S (10 mg/ml) at room temperature for 45 minutes. The cell layers were then washed with distilled water five times and dried completely. Stained cell layers were photographed using a Zeiss Axiovert 200 microscope (Carl Zeiss Microimaging, Thornwood, NY). Quantitative calcium mineral contents were measured by a de-staining procedure using an extraction solvent containing a mixture of 10 % acetic acid and methanol at room temperature for 30 minutes. 200 µL aliquots of alizarin red S extracts were then added in a 96-well assay plate. The Alizarin Red S concentrations of the samples and standard was determined at the absorbance at 405 nm (TECAN Infinite F50) and expressed as µg/ml.

2.6. *In vivo* study

2.6.1. Animals and surgery

All animal experiments were performed in accordance with the protocol approved by the Institutional Animal Care and Use Committee. There were five experimental groups with increasing doses of BMP-2 included in the CLF gel (0 µg, 0.5 µg, 1 µg, 2 µg and 5 µg). The procedure for creation of a critical-sized femoral defect in Sprague-Dawley rat has been previously described [27]. Briefly, unilateral critical sized, 6mm segmental defects were created in the right femur of 30 adult, male Sprague-Dawley rats. The rats weight ranged from 354 to382 grams (Harlan Laboratories). The right hindlimb was shaved and prepared for surgery in an aseptic fashion. A longitudinal incision was made inline with the femoral diaphysis and carried

down to the bone. Once the femur was exposed, a polyacetyl plate (27mm long x 4 mm wide x 4 mm thick) was fixed to the lateral aspect of the femur and held in place with 6 bicortical, threaded wires. A 6mm segment of bone was then removed for the mid-diaphyseal region of the femur using a reciprocating saw to make the osteotomies. The wound was irrigated and dried. The CLF gel was then placed into the defect (Fig. 1a). The wound was then closed with suture and staples. Post-surgery, the animals were allowed full activity in their cages. They were survived for 4 weeks post-surgery and then were euthanized. The right femurs were then harvested with the plate fixation intact. The soft tissue around each femur was removed; specific care was taken not to disturb the defect site. The femurs were stored in 10% neutral buffered formalin.

2.6.2. X-ray radiograph

2-dimensional radiographic imaging was performed using a Faxitron x-ray system (Faxitron X-ray Corporation [Model: MX-20], Tucson, Arizona; time 15s, 35 kV). It was used to confirm appropriate position of the plate and wires immediately post-operatively (Fig. 1b) and to evaluate bone growth from week 0 to week 4. At week 4 the sample was considered to have bridging bone if there was continuous bone at both of the proximal and both of the distal junctions between the cortex and the defect.

2.6.3. Microcomputed tomography (micro CT) analysis

The samples underwent *ex vivo* micro CT scans at 4 weeks using a VivaCT 40 (Scanco Medical, Brüttisellen Switzerland). It was set at 55 kV source voltage, 145 μA source current, and a resolution of 21 microns. The images were reconstructed using NRecon software (Bruker Biospin Corp, Billerica, MA). The region of interest (ROI) included the entire 6 mm defect. The threshold was set at 876 mg/cm^3 (corresponding to 73 on a scale of 0-255) to define mineralized

tissue across all samples in the study [28]. CTAn software (Skyscan, Bruker Biospin Corp, Billerica, MA) was used to analyze the images.

2.6.4. Histological staining

After μCT analysis at 4 weeks of implantation, the femoral segmental defect specimens were taken for histological staining. The samples were fixed with 10% neutral buffered formalin (NBF), decalcified in 10% Ethylene Diamine Tetraacetic Acid (EDTA), dehydrated in graded ethanol solutions (70%-100%), and embedded in paraffin. Serial sections of the samples (4 μm thick) were stained with Hematoxylin & Eosin (H&E).

2.9. Statistical analysis

All data are presented as mean ± standard deviation. Presence of significant outliers in the data set was identified by using the Grubb's test (Graphpad Software Inc, La Jolla, CA). Significant differences were analyzed by one-way ANOVA test, the Kruskal-Wallis test for ANOVA on ranks or Fisher's exact test for categorical data (SigmaPlot 12.0, Systat Software Inc, San Jose, CA). The differences in groups and experimental time points at any time were considered significant if $p<0.05$.

3. Results

3.1. Characterization of CLF hydrogels

3.1.1. FTIR spectra

Changes in the chemical structure after incorporation of fibrinogen were confirmed by FTIR spectra (Fig. 2). The spectrum of the CL exhibited characteristic peaks of both chitosan and lactide which were attributed to the C=O stretching vibrations of amide I at 1620 cm^{-1}, the N-H bending vibrations of amide II at 1548 and 1589 cm^{-1}, and the C-N bending of the amine groups at 1261 cm^{-1}. The peaks at 1031 cm^{-1} and 1074 cm^{-1}, representative of the C-O-C bending of the

chitosan, were observed. The peaks at 1379, 1409, and 1460 cm^{-1} were the characteristic band of CH_3 symmetrical deformation. The absorption at 1741, 1784, and 1820 cm^{-1} are probably attributed to C=O stretching vibrations owing to the overlapping of the peaks from N-acetyl groups in the chitosan and the ester that coupled the chitosan and lactide.

Compared to the IR spectrum of CL, the intensity of amide I in CLF was enhanced at 1631 cm^{-1} after incorporation of fibrinogen [29-30]. It is the major spectral feature in native fibrinogen. The peaks ascribed to the N-H bending vibrations of amide II were also enhanced and shifted to 1548 cm^{-1} from 1589 cm^{-1}, indicating that the amount of amide group increased in the copolymer. The complex bands of amide III were observed at 1330 cm^{-1} attributable to coupling of side chains and hydrogen bonding of the fibrinogen with hydroxyl or amino groups in the structure of copolymer. The CLF signal intensity of the CH_3 mode at 1409 cm^{-1} increased with the fibrinogen molecules due to increased content of amino acids. This evidence suggests that fibrinogen can react with the chitosan-lactide copolymer.

3.1.2. SEM observations

Figure 2 shows representative SEM images of the cross-section for lyophilized CL and CLF hydrogels. All hydrogels showed homogeneous and microporous structures throughout the cross-section. The CL hydrogel (Fig. 3a and 3c) exhibited relatively smooth and flat surfaces formed by the combination of chitosan and lactide. Figure 3b and 3d show protein aggregation on the surface of the CLF hydrogel. This aggregation of the protein molecules is due to the formation of intermolecular hydrogen bonds between hydroxyl and amino groups of chitosan-lactide copolymer and fibrinogen molecules [29].

3.1.3. Mechanical testing

The effect of UV exposure times on compressive modulus of the CLF hydrogels was determined (Fig. 4a). The compressive moduli of the CLF hydrogels increased with increasing

UV cross-linking time. CLF hydrogels possessed 4.4 ± 1.2, 14.4 ± 2.0, 15.7 ± 0.9, 29.9 ± 0.7, 29.2 ± 1.5, and 31.7 ± 0.9 kPa of compressive modulus at 50s, 100s, 150s, 200s, 250s, and 300s of UV exposure time, respectively. 200s of UV exposure appeared to almost reach maximal strength of the CLF hydrogels, even though there was still a significant difference between 200s and 300s. It is worth mentioning that some structural failures were observed in the hydrogels at 300s of UV irradiation for strain range of 20-30%, indicating the decreased flexibility and increased stiffness of the hydrogels at a longer UV exposure time. In addition, the average compressive modulus (Fig. 4b) for CLF hydrogels at 200s of UV exposure time was 29.9 ± 0.7 kPa, which was significantly greater than the modulus for CL hydrogels at 22.7 ± 1.7 kPa (p<0.05). The results showed that addition of fibrinogen molecules increased the compressive modulus of the hydrogels.

3.1.4. *In vitro* degradation characteristics

To understand the influence of different pHs and enzymatic activities on the degradation behaviors, the wet remaining ratios of CL and CLF hydrogels were examined after incubating them in PBS (pH 7.4), PBS (pH 4), or 1mg/ml collagenase A containing PBS (pH 7.4) at 37°C (Fig. 5). In the PBS (pH 7.4) medium, the wet weight remaining ratio of the CL hydrogels was similar to that of the CLF hydrogels for a 4-week incubation. The shape of both hydrogels was well maintained, and the wet weight remaining ratio slowly decreased to 83.82% for the CL and 83.62% for the CLF after 4 weeks incubation, respectively. In the PBS (pH 4) medium, both hydrogels showed significant increases in wet weight remaining ratio after 1 day of the incubation (p<0.05), indicating the acidic condition induced the absorption of a greater amount of water. In the 1 mg/ml collagenase A containing PBS solution, the wet weight remaining ratios significantly decreased to 78.4% for the CL and 78.9% for the CLF after 1 day of the incubation (p<0.05) and then slowly decreased over a 4-week period. The result demonstrated that the swelling and

degradation behaviors of the chitosan-lactide hydrogels were influenced by pHs and enzymatic activities.

3.2. *In vitro* release study of BMP-2

The *in vitro* release behaviors of BMP-2 from the CLF hydrogels were interpreted by the cumulative amount and percentage of the BMP-2 as a function of time. Figure 6a and 6b show the cumulative release of the BMP-2 from the CLF hydrogels. The CLF hydrogels containing a higher concentration (100 ng/ml) of BMP-2 released significantly greater amounts compared with the gels containing a lower concentration (10 ng/ml) for a 4-week period. The CLF hydrogels containing a higher concentration (100 ng/ml) of BMP-2 showed an initial burst release of 24% of the total amount within 1 day followed by a slow release of 71% of the total amount over the 4-week incubation. Similarly, the CLF hydrogels containing a lower concentration (10 ng/ml) of BMP-2 exhibited initial burst release of 35% of the total amount within 1 day and sustained release of 60% of the total amount over the 4-week incubation. However, there was no significant difference in the release profiles by percentages for the hydrogels with the higher or lower amounts of BMP-2. The result demonstrated initial burst releases of the BMP-2 from the CLF hydrogels followed by sustained releases, regardless of the concentration of the protein.

3.3. *In vitro* bioactivities

3.3.1. Cytotoxicity of CLF hydrogels

The cytotoxicity of the hydrogels was examined by a MTS assay using the W-20-17 and C2C12 cells, and the changes in the cell morphology were observed by a microscope for 3 days of incubation. As shown in Figure 7, there were significant increases in metabolic activity of W-20-17 and C2C12 cells after 3 days of culture ($p<0.05$). Cells in all the groups showed significantly higher metabolic activity and were highly confluent at day 3 than day 1 ($p<0.05$), indicating the non-cytotoxicity of the hydrogels. However, there was no significant difference

between the groups for 3 days of incubation. The result demonstrated that different concentration of BMP-2 did not significantly affect cell growth and proliferation. Consistent with a MTS assay, the microscopic imaging shows cells in all the groups significantly proliferated for 3 days of culture (Fig. 7c and 7d), suggesting cells were viable in the presence of the hydrogels regardless of BMP-2 incorporation.

3.3.2. ALP production in response to BMP-2

ALP specific activity was assessed as an early indicator of the osteoblastic lineage to study the effect of BMP-2 on osteoblast differentiation. W-20-17 and C2C12 cells were cultured with the CLF hydrogels containing different concentrations of BMP-2, and their ALP specific activities were determined by normalizing the ALP amount to the dsDNA content per sample at day 7. Figure 8a shows ALP specific activity of the W-20-17 treated with different concentration of BMP-2. Significant differences in ALP specific activity were observed among the various concentration of BMP-2. At 7 days of cell culture, the W-20-17 treated with BMP-2 via the CLF hydrogel expressed significantly higher ALP activity ($p<0.05$) compared with the hydrogel alone (0 ng/ml of BMP-2). ALP specific activity of the W-20-17 was significantly increased with the BMP-2 loaded CLF hydrogels in a concentration-dependent manner ($p<0.05$). As shown in Figure 8b, the highest ALP expression in the C2C12 cells was also found in the CLF hydrogels containing 500 ng/ml of BMP-2 during 7 days of cell culture. The C2C12 exhibited the lowest ALP expression in the group that did not contain BMP-2 ($p<0.05$). However, there was no significant difference between the hydrogels containing 50 ng/ml and 100 ng/ml BMP-2. Both the W-20-17 and C2C12 cells expressed significantly higher ALP activities in response to a higher concentration of BMP-2.

3.3.3. Mineralization stained by Alizarin Red S

The dose effect of BMP-2 on mineralization and nodule formation in W-20-17 and C2C12 cells was investigated by staining with a 1% Alizarin Red S. Quantitative levels of calcium mineral content were measured by a destaining procedure. In the cultures of the W-20-17 (Fig. 9a), the CLF hydrogel without BMP-2 showed no positive Alizarin Red S staining for 21 days, suggesting that the W-20-17 cells did not differentiate into a mineralized phenotype without BMP-2 supplementation for 21 days. However, in the presence of BMP-2, significant Alizarin Red S staining was apparent in cultures treated with the CLF hydrogels containing BMP-2 in a dose- and time-dependent manner ($p<0.05$). The highest calcium accumulation occurred in cultures treated with the CLF hydrogels containing 500ng/ml of BMP-2 at 21 days.

In the C2C12 cultures (Fig. 9b), calcium mineral formation in all groups significantly increased at day 21 compared with day 10 ($p<0.05$). In the CLF hydrogels without BMP-2, calcium deposition increased in a time dependent manner, but there was very little staining with a small number of mineralized bone nodules at day 21 formed along with the cell layer. The highest calcium accumulation was observed in cultures treated with the hydrogels containing 500ng/ml of BMP-2 at 21 days.

3.4. *In vivo* study

3.4.1 X-ray radiographs

All 30 rats survived the full length of the study. Figure 10 shows representative x-ray radiographs at week 2 and 4. Bridging bone across the defect was not evident in any of the femurs in the 0 μg BMP-2 CLF hydrogel group and only one of the femurs in the 0.5 μg BMP-2 group. There was a trend toward an increased rate of bridging in the 1 μg, 2 μg and 5μg groups (4 femurs bridged in each group) compared to the 0 μg and 0.5 μg groups ($p = 0.06$ and $p = 0.24$ respectively).

3.4.2 Micro CT scan and analysis

Figure 11 shows the representative Micro CT scan (Fig. 11a) and analysis (Fig. 11b).Micro CT analysis of the samples demonstrated a dose response with an increase in the amount of bone volume (BV) with increasing amounts of BMP-2 in the CLF hydrogel. It was found that the BV regenerated was significantly greater at the 5 µg BMP-2 dose compared to the group with no BMP-2 ($p<0.05$). The largest interval increase in bone volume was seen with the increase of BMP-2 from 0.5 µg to 1 µg (52% increase), and 1 to 2 µg (35% increase) BMP-2 in the CLF hydrogel.

3.4.3. Histological staining

To further investigate BMP-mediated bone formation, histological imaging of longitudinal cross-sections of samples was taken at 4 weeks after surgery. Figure 12 exhibits the robust new bone formation induced by the BMP-2 containing CLF hydrogels in the critical size bone defects, including osteoblasts, osteocytes embedded in newly deposited bone matrix, multinucleated osteoclast-like cells, and blood vessels. The CLF hydrogels were partially degraded, but could still be detected within and around the defects.

The CLF hydrogel alone group exhibited massive infiltration of cells, but very little new bone formation. Few newly formed bones were observed in the proximity of segment ends of native bone (Fig. 12a). However, extensive new bone formation was clearly observed in the periphery of the CLF hydrogels containing BMP-2 corresponding to cortical shell of long bone, and started to bridge the longitudinal bone gaps with the increasing doses of BMP-2, which were consistent with the radiographic and µCT results. More specifically, in the CLF hydrogels (0.5 µg BMP-2), H&E staining revealed a bony structure with the capping of the segment ends that extended beyond the defect. The extent of trabecular bone in the CLF hydrogel group (0.5 µg BMP-2) was moderately more than that in the CLF hydrogel alone, without a bone defect bridging. On the other hand, in the defects implanted with the CLF hydrogels with increasing amounts of BMP-2 (1, 2, and 5µg), more pronounced bone formation was observed, including

bone bridges and trabecular bony structures that were filled with newly formed bone marrow cellularity. As shown in Figure 12b, at a higher magnification, osteocytes were embedded in a new bone, and osteoblasts lined along the new bone surface inside the defect region.

Discussion

In the present study, we have developed and characterized a hydrogel platform system for the delivery of BMP-2 and validated its effectiveness by repairing critical size rat femoral defects. The CLF hydrogels were synthesized by reacting D,L-lactide onto chitosan, followed by incorporation of fibrinogen. The prepolymer solution of the CLF hydrogel forms photo-cross-linkable copolymer networks via a radical polymerization upon application of UV light. In our hydrogel systems, the hydrophilic chitosan backbone molecules and hydrophobic polylactide side chains can form the copolymer networks with both hydrophobic and hydrophilic components, which can be suitable for delivery of variety of drugs regardless of wettability. Furthermore, amide or ester linkages for the branched PLA chains can function as plasticizers internally in the rigid main chain of chitosan [31-32], providing the mechanical flexibility and elasticity of the hydrogel [24]. Another significant advantage of the CLF hydrogel system is that growth factor binding ligands such as fibrinogen can be easily incorporated into the prepolymer solution due to the hydrophilic nature of chitosan. The heparin-binding domains of fibrinogen can bind a wide range of growth factors including BMP-2 and potentially promotes tissue repair when incorporated within a synthetic matrix [20-23, 33].

In this study, the chemical and structural changes were observed by FTIR spectra and SEM images. The CL hydrogels were formed by the interactions between carbonyl groups of the lactide, and hydroxyl and amine groups of the chitosan. With addition of fibrinogen, homogeneous protein aggregation was observed on the surface of the CLF hydrogel, resulting from the interaction between residues of the fibrinogen and hydroxyl or amino groups in the CL copolymer [29-30]. As a result, the changes in the chemical and structural properties influenced

mechanical properties, degradation behaviors, and BMP-2 release kinetics. The compressive moduli of the CLF hydrogels suggested that a longer UV exposure time reinforced microstructure of the hydrogels due to increased degree of cross-linking. However, some structural failures were observed in the hydrogels for strain range of 20-30% at 300s of UV irradiation. This indicated that there is a suitable range of stiffness and elasticity of the hydrogels at appropriate UV exposure time for possible clinical applications. Addition of fibrinogen molecules also increased the elasticity of the co-polymer networks, due to the effect of intermolecular hydrogen bonds between hydroxyl and amino groups of chitosan-lactide copolymer and fibrinogen molecules [22-23]. This result was consistent with Jiang *et al*.'s report that the presence of fibrin increased stiffness of porous PEG hydrogels relative to control porous hydrogels, and the compressive modulus of the hydrogels increased with the concentration of the fibrinogen [22]. In the in vivo study, the CLF hydrogels using 200s of UV was selected because the CLF hydrogels were mechanically sufficient to be press-fitted into the critical size segmental defects in femur while remaining structural integrity and stabilizing interface, potentially enhancing bone bridging and regeneration as a promising synthetic bone substitute [1, 33].

Swelling behavior and degradation profile of both CL and CLF hydrogels were affected by pHs and enzymatic activities in medium and/or microenvironment. We used neutral and acidic pHs to mimic physiological and fresh bony fracture trauma conditions [34]. Acidic condition resulted in significantly greater swelling of both hydrogels compared to neutral pH environment. This is because the acidic condition increased the mobility of the hydrogel chains. Consequently, the hydrogel increased its ability to absorb water. An addition of collagenase into PBS significantly accelerated the degradation of both CL and CLF hydrogels within 1 day of the incubation, but the overall degradation rates were slow. This is because the collagenase, a member of the matrix metalloproteinase (MMP) family, proteolyzes plasma proteins such as fibrinogen [35], but not specifically on the chitosan backbones. Generally, the fraction of N-acetylglucosamine (NAG) units in chitosan contributes to its enzymatic hydrolysis [36].

Previously, we have demonstrated that the presence of lysozyme significantly accelerated degradation rates of the CL hydrogels compared with those in absence of lysozyme [24]. The enzymatic degradation rate of the hydrogels was tunable regarding composition and the degree of cross-linking of the hydrogels, as well as the medium/microenvironment which the hydrogels are in contact with.

In order to study the dose effect of BMP-2 on bone formation, we incorporated different doses of BMP-2 into the CLF hydrogels and investigated BMP-2 release kinetics *in vitro*. Our i*n vitro* release study demonstrated initial burst releases of the BMP-2 from the CLF hydrogels followed by sustained releases regardless of the concentration of the BMP-2. The initial burst release is mainly due to rapid release of BMP-2 absorbed on the surface of the hydrogel and diffusion via swelling [37-39]. The sustained release is regulated by intermolecular interactions between the proteins and hydrogels, as well as degradation behaviors [38, 40]. In our previous study, we found that a higher degree of cross-linking via a longer UV irradiation significantly reduced the initial burst release and extended the release periods of BSA from the chitosan-lactide hydrogels [24].

We first evaluated the in vitro cytotoxicity of hydrogels loaded with BMP-2 by observing the changes in cell metabolic activity and cell morphology. The W-20-17 cell line was selected because it has been used for an ASTM (F2131) standard test for *in vitro* biological activity of BMP-2 [41-42]. The C2C12 was also selected because BMP-2 can induce transdifferentiation of C2C12 myoblasts into osteoblasts [43, 44]. Both W-20-17 and C2C12 cells were viable in the presence of the hydrogels regardless of BMP-2 doses, indicating the non-cytotoxicity of the hydrogels. Furthermore, we investigated the dose effect of BMP-2 on osteoblast differentiation and mineralization. The greater ALP activity of both W-20-17 and C2C12 cells was observed in the presence of the CLF hydrogels containing the highest dose (500 ng/ml) of BMP-2 at day 7. It is most likely that the CLF hydrogels with BMP-2 (500 ng/ml) released greater amounts of BMP-2 than the others at the time period. Similarly, significantly greater amount of mineralization and

nodule formation in both W-20-17 and C2C12 cells were apparent in cultures treated with the CLF hydrogels containing BMP-2 in a dose- and time-dependent manner ($p<0.05$). It is worth noting that cell responses to BMP-2 are highly variable depending on cell types and different phases of phenotype maturation.

Our *in vivo* results also demonstrated that BMP-2 loaded into the CLF hydrogels enhanced neo-osteogenesis and accelerated healing of the bone defects in a dose-dependent manner. Addition of high dose of BMP-2 (1, 2, and 5μg) to the CLF hydrogels prompted considerably more bone formation than the CLF hydrogel alone or containing low concentration of BMP-2 (0.5μg), indicating successful and effective CLF hydrogel-mediated delivery of BMP-2 to the defect site. In fact, the bone volume regenerated at the 5 μg dose of BMP-2 was significantly greater than that regenerated with the CLF hydrogel alone. In addition, we did not observe any inflammatory response nor any adverse side effect inducing abnormal bone structure and cellularity in the range of BMP-2 doses we used. In nature, inflammation is inherent part of wound healing and tissue regeneration [45, 46, 47]. The intensity of the inflammatory responses could be mitigated by manipulating chemical composition and degradation of the biomaterials [45, 47]. We have demonstrated that adjustment of the ratios of chitosan to lactide modulated degradation rates, protein adsorption, and release kinetics of chitosan-lactide copolymer [24]. In addition, Santos et al. revealed pro-inflammatory and pro-healing roles of fibrinogen in chitosan scaffolds. The fibrinogen incorporation showed enhanced bone formation and stimulated angiogenesis even though it elicited immune response [47]. Peled et al. also demonstrated that PEGylated fibrinogen material can promote the healing of bone defects and sustained release of fibrinogen fragments induce bone regeneration at the injury site [48]. As such, the use of fibrinogen molecules can be more effective when combined with appropriate biomaterials which provide structural support and maintain biological functionality compared to conventional fibrin mediated bone applications. In this regard, incorporation of fibrinogen molecules into the CL

hydrogels could reduce a risk of inflammation and enhance bone healing in combination of appropriate dose of BMP-2.

Previous studies have reported that BMP-2 can induce adverse side effects such as cyst-like bone formation and significant soft tissue swelling when treated with high doses [11, 13, 49]. Janette *et al.* reported that high doses of BMP-2 (11.25, 22.5, and 45 µg) loaded into PLGA scaffolds induced structurally abnormal bone and inflammation in a rat femoral segmental defect model, whereas normal trabecular architecture and bone marrow cellularity were observed with BMP-2 (2.25 µg) [5]. This low dose result was consistent with our finding in normal bone formation (0-5 µg). The adverse outcome of higher doses of BMP-2 is most likely due to a threshold of BMP-2 for enhancing bone healing. The excessive dose of BMP-2 may induce excessive inflammation and lead to rather lower quality of bone formation. Therefore, it is important to use physiologically relevant dose of BMP-2 for specific species and a delivery system that allows a controlled and sustained release for high quality of bone formation [5, 45]. As the goal of this study was to evaluate dose effect and establish a suitable dose of BMP-2 using our newly developed hydrogels in a rat femoral segmental defect model for 4 weeks. In future research, we will investigate the effect of a controlled and sustained release of BMP-2 from the CLF hydrogel in a rat femoral segmental defect model for a long term in comparison with a commercially available collagen sponge.

Conclusions

We have shown in the present study that our photo-cross-linkable CLF hydrogel can effectively deliver BMP-2 to regulate cell response and enhance osteogenesis both *in vitro* and *in vivo*. Incorporation of fibrinogen molecules affected structural and mechanical properties as well as degradation profiles of the hydrogels. The BMP-2 containing CLF hydrogels exhibited an initial burst release followed by a sustained release of BMP-2 over 4 weeks, and enhanced neo-osteogenesis and accelerated healing of the bone defect in a dose-dependent manner. However, it

is worth noting that combination of physiologically acceptable dose of BMP-2 and its controlled and sustained release can improve quality of bone formation and avoid adverse side effects associated with high dose.

Acknowledgments

We acknowledge the grant supports from DOD W81XWH-10-1-0966, Airlift Research Foundation, Wallace H. Coulter Foundation, NIH R01AR057837 from NIAMS and NIH R01DE021468 from NIDCR.

References

1. Harris JS, Bemenderfer TB, Wessel AR, Kacena MA. A review of mouse critical size defect models in weight bearing bones. Bone 2013:55;241-7.

2. Axelrad TW, Einhorn TA. Bone morphogenetic proteins in orthopaedic surgery. Cytokine Growth Factor Rev 2009:20;481-8.

3. Yu YY, Lieu S, Lu C, Colnot C. Bone morphogenetic protein 2 stimulates endochondral ossification by regulating periosteal cell fate during bone repair. Bone 2010:47;65-73.

4. Schu¨tzenberger S, Schultz A, Hausner T, Hopf R, Zanoni G, Redl H, et al. The optimal carrier for BMP-2: a comparison of collagen versus fibrin matrix. Arch Orthop Trauma Surg 2012:132;1363-70.

5. Zara JN, Siu RK, Zhang X, Shen J, Ngo R, Soo C, et al. High doses of bone morphogenetic protein 2 induce structurally abnormal bone and inflammation in vivo. Tissue Eng Part A 2011:17;1389-99.

6. Martino M, Tortelli F, Mochizuki M, Traub S, Ben-David D, Hubbell JA, et al. Engineering the growth factor microenvironment with fibronectin domains to promote wound and bone tissue healing. Sci Transl Med 2011:3(100);1-8.

7. Schmidmaier G, Schwabe P, Strobel C, Wildemann B. Carrier systems and application of growth factors in orthopaedics. Injury, Int. J. Care Injured 2008;39S2:S37-S43.

8. McKay WF, Peckham SM, Badura JM. A comprehensive clinical review of recombinant human bone morphogenetic protein-2 (INFUSE® Bone Graft). Int Orthop. 2007;31(6):729-34.

9. White AP, Vaccaro AR, Hall JA, Whang PG, Friel BC, McKee MD. Clinical applications of BMP-7/OP-1 in fractures, nonunions and spinal fusion. Int Orthop. 2007;31(6):735-41.

10. Bhakta G, Rai B, Lim ZXH, Hui JH, Stein GS, van Wijnen AJ, et al. Hyaluronic acid-based hydrogels functionalized with heparin that support controlled release of bioactive BMP-2. Biomaterials 2012;33:6113-22.

11. Ben-David D, Srouji S, Shapira-Schweitzer K, Kossover O, Ivanir E, Livne E, et al. Low dose BMP-2 treatment for bone repair using a PEGylated fibrinogen hydrogel matrix. Biomaterials 2013;34:2902-10.

12. Schmoekel HG, Weber FE, Schense JC, Grätz KW, Schawalder P, Hubbell JA. Bone repair with a form of BMP-2 engineered for incorporation into fibrin cell ingrowth matrices. Biotechnol Bioeng 2005;89(3):253-62.

13. Bhakta G, Lim ZX, Rai B, Lin T, Hui JH, Cool SM, et al. The influence of collagen and hyaluronan matrices on the delivery and bioactivity of bone morphogenetic protein-2 and ectopic bone formation. Acta Biomater. 2013 doi: 10.1016/j.actbio.2013.07.008.

14. Mariner PD, Wudel JM, Miller DE, Genova EE, Streubel SO, Anseth KS. Synthetic hydrogel scaffold is an effective vehicle for delivery of INFUSE (rhBMP2) to critical-sized calvaria bone defects in rats. J Orthop Res 2013;31(3):401-6.

15. Vo TN, Kasper FK, Mikos AG. Strategies for controlled delivery of growth factors and cells for bone regeneration. Adv Drug Deliv Rev 2012;64:1292-309.

16. Jeon O, Powell C, Solorio LD, Krebs MD, Alsberg E. Affinity-based growth factor delivery using biodegradable, photocrosslinked heparin-alginate hydrogels. J Control Release. 2011;154(3):258-66.

17. Sakiyama-Elbert SE, Hubbell JA. Development of fibrin derivatives for controlled release of heparin-binding growth factors. J Control Release 2000;65(3):389-402.

18. Gandhi NS, Mancera RL. Prediction of heparin binding sites in bone morphogenetic proteins (BMPs). Biochim Biophys Acta. 2012;1824(12):1374-81.

19. Ruppert R, Hoffmann E, Sebald W. Human bone morphogenetic protein 2 contains a heparin-binding site which modifies its biological activity. Eur J Biochem 1996;237(1):295-302.

20. Odrljin TM, Shainoff JR, Lawrence SO, Simpson-Haidaris PJ. Thrombin cleavage enhances exposure of a heparin binding domain in the N-terminus of the fibrin beta chain. Blood. 1996;88(6):2050-61.

21. Martino MM, Briquez PS, Ranga A, Lutolf MP, Hubbell JA. Heparin-binding domain of fibrin(ogen) binds growth factors and promotes tissue repair when incorporated within a synthetic matrix. Proc Natl Acad Sci U S A 2013;110(12):4563-8.

22. Jiang B, Waller TM, Larson JC, Appel AA, Brey EM. Fibrin-loaded porous poly(ethylene glycol) hydrogels as scaffold materials for vascularized tissue formation. Tissue Eng Part A. 2013;19(1-2):224-34.

23. Shikanov A, Xu M, Woodruff TK, Shea LD. Interpenetrating fibrin-alginate matrices for in vitro ovarian follicle development. Biomaterials. 2009;30(29):5476-85.

24. Kim S, Kang Y, Mercado-Pagán AE, Maloney WJ, Yang Y. In vitro evaluation of photo-crosslinkable chitosan-lactide hydrogels for bone tissue engineering. J Biomed Mater Res B Appl Biomater. 2014. doi: 10.1002/jbm.b.33118.

25. Xu X, Jha AK, Duncan RL, Jia X. Heparin-decorated, hyaluronic acid-based hydrogel particles for the controlled release of bone morphogenetic protein 2. Acta Biomater. 2011;7(8):3050-9.

26. Praveen G, Sreerekha PR, Menon D, Nair SV, Chennazhi KP. Fibrin nanoconstructs: a novel processing method and their use as controlled delivery agents. Nanotechnology. 2012;23(9):1-11.

27. Patel ZS, Young S, Tabata Y, Jansen JA, Wong ME, Mikos AG. Dual delivery of an angiogenic and an osteogenic growth factor for bone regeneration in a critical size defect model. Bone. 2008;43(5):931-40. doi: 10.1016/j.bone.2008.06.019.

28. Brown KV, Li B, Guda T, Perrien DS, Guelcher SA, Wenke JC. Improving bone formation in a rat femur segmental defect by controlling bone morphogenetic protein-2 release. Tissue Eng Part A. 2011;17(13-14):1735-46. doi: 10.1089/ten.

29. Litvinov RI, Faizullin DA, Zuev YF, Weisel JW. The α-helix to β-sheet transition in stretched and compressed hydrated fibrin clots. Biophys J. 2012;103(5):1020-7.

30. Shrivastava S, Singh SK, Mukhopadhyay A, Sinha AS, Mandal RK, Dash D. Negative regulation of fibrin polymerization and clot formation by nanoparticles of silver. Colloids Surf B Biointerfaces. 2011;82(1):241-6.

31. Liu Y, Tian F, Hu KA. Synthesis and characterization of a brush-like copolymer of polylactide grafted onto chitosan. Carbohydr Res. 2004;339(4):845-51.

32. Wu Y, Zheng Y, Yang W, Wang C, Hu J, Fu S. Synthesis and characterization of a novel amphiphilic chitosan–polylactide graft copolymer. Carbohydr Polym 2005;59:165-71.

33. Falvo MR, Gorkun OV, Lord ST. The molecular origins of the mechanical properties of fibrin. Biophys Chem. 2010;152(1-3):15-20.

34. Barrère F, van Blitterswijk CA, de Groot K. Bone regeneration: molecular and cellular interactions with calcium phosphate ceramics. Int J Nanomedicine. 2006;1(3):317-32.

35. Hiller O, Lichte A, Oberpichler A, Kocourek A, Tschesche H. Matrix metalloproteinases collagenase-2, macrophage elastase, collagenase-3, and membrane type 1-matrix metalloproteinase impair clotting by degradation of fibrinogen and factor XII. J Biol Chem 2000;275(42):33008-13.

36. Freier T, Koh HS, Kazazian K, Shoichet MS. Controlling cell adhesion and degradation of chitosan films by N-acetylation. Biomaterials. 2005;26(29):5872-8.

37. An J, Yuan X, Luo Q, Wang D. Preparation of chitosan-graft-(methyl methacrylate)/Ag nanocomposite with antimicrobial activity. Polym Int 2010;59:62-70.

38. Pitarresi G, Casadei MA, Mandracchia D, Paolicelli P, Palumbo FS, Giammona G. Photocrosslinking of dextran and polyaspartamide derivatives: a combination suitable for colon-specific drug delivery. J Control Release 2007;119(3):328-38.

39. Guo BL, Gao QY. Preparation and properties of a pH/temperature-responsive carboxymethyl chitosan/poly(N-isopropylacrylamide)semi-IPN hydrogel for oral delivery of drugs. Carbohydr Res 2007;342(16):2416-22.

40. Hong Y, Song H, Gong Y, Mao Z, Gao C, Shen J. Covalently crosslinked chitosan hydrogel: properties of in vitro degradation and chondrocyte encapsulation. Acta Biomater. 2007;3(1):23-31.

41. Nguyen AH, Kim S, Maloney WJ, Wenke JC, Yang Y. Effect of coadministration of vancomycin and BMP-2 on cocultured Staphylococcus aureus and W-20-17 mouse bone marrow stromal cells in vitro. Antimicrob Agents Chemother 2012;56(7):3776-84.

42. Kempen DH, Lu L, Hefferan TE, Creemers LB, Maran A, Yaszemski MJ, et al. Retention of in vitro and in vivo BMP-2 bioactivities in sustained delivery vehicles for bone tissue engineering. Biomaterials. 2008;29(22):3245-52.

43. Bramono DS, Murali S, Rai B, Ling L, Poh WT, Cool SM, et al. Bone marrow-derived heparan sulfate potentiates the osteogenic activity of bone morphogenetic protein-2 (BMP-2). Bone 2012;50(4):954-64.

44. Katagiri T, Yamaguchi A, Komaki M, Abe E, Takahashi N, Suda T, et al. Bone morphogenetic protein-2 converts the differentiation pathway of C2C12 myoblasts into the osteoblast lineage. J Cell Biol 1994;127(6 Pt 1):1755-66.

45. Mountziaris PM, Spicer PP, Kasper FK, Mikos AG. Harnessing and modulating inflammation in strategies for bone regeneration. Tissue Eng Part B Rev 2011;17(6):393-402.

46. Barbosa JN, Amaral IF, Aguas AP, Barbosa MA. Evaluation of the effect of the degree of acetylation on the inflammatory response to 3D porous chitosan scaffolds. J Biomed Mater Res A. 2010;93(1):20-8.

47. Santos SG, Lamghari M, Almeida CR, Oliveira MI, Neves N, Barbosa MA et al. Adsorbed fibrinogen leads to improved bone regeneration and correlates with differences in the systemic immune response. Acta Biomater. 2013;9(7):7209-17.

48. Peled E, Boss J, Bejar J, Zinman C, Seliktar D. A novel poly(ethylene glycol)-fibrinogen hydrogel for tibial segmental defect repair in a rat model. J Biomed Mater Res A. 2007;80(4):874-84.

49. Sciadini MF, Johnson KD. Evaluation of recombinant human bone morphogenetic protein-2 as a bone-graft substitute in a canine segmental defect model. J Orthop Res 2000;18(2):289-302.

Figure Legends

Figure 1 (a) Digital micrograph of a critically sized rat femoral defect after placement of a CLF hydrogel (dotted circles). (b) Representative radiograph of the bone defects with implantation of CLF hydrogels immediately post-operatively.

Figure 2 FTIR spectra of prepolymer solution of chitosan-lactide (CL) and chitosan-lactide-fibrinogen (CLF).

Figure 3 SEM micrographs of cross-section for lyophilized (a) CL hydrogel; (b) CLF hydrogels; (c) high magnification of CL; (d) high magnification of CLF. Samples were incubated at 37°C for 1day and lypholized overnight before the examination under a scanning electron microscope (FEI XL30 Sirion SEM) operated at 5 kV voltages.

Figure 4 Compressive modulus of hydrogels according to (a) different UV exposure times on the CLF hydrogel; (b) the presence of fibrinogen. Unconfined compression tests were performed using an Instron 5944 materials testing system fitted with a 10 N load cell. The compressive modulus was determined for strain ranges of 10-20% from linear curve fits of the stress-strain curve. Each value represents the mean ± SD (n = 3). * denotes significant difference between groups at same UV exposure time (p<0.05).

Figure 5 *In vitro* degradation of hydrogels in (a) PBS (pH 7.4); (b) PBS (pH 4); (c) PBS (pH 7.4) containing collagenase A (1mg/ml) at 37°C for 28 days. The degradation profile of the hydrogels was determined by measuring the wet remaining ratio of the hydrogels at each time point. Each value represents the mean ± SD (n = 3).

Figure 6 *In vitro* cumulative release profiles of BMP-2 from CLF hydrogels over a 4-week period. The cumulative release (a) amount and (b) percentage of BMP-2 from the CLF hydrogels were determined as a function of time by a BMP-2 immunoassay at 450 nm. Concentration of BMP-2 was 10 or 100 ng/ml. Each value represents the mean ± SD (n = 3 per each group).

Figure 7 Cytotoxicity of CLF hydrogels containing different concentrations of BMP-2 (0, 50, 100, or 500 ng/ml) using W-20-17 preosteoblast mouse bone marrow stromal cells and C2C12 mouse myoblast cells. (a) Viability of W-20-17 via an MTS assay; (b) Viability of C2C12 via an MTS assay; (c) Photomicrographs of the morphology of W-20-17; (d) Photomicrographs of the morphology of C2C12. The cells were seeded at a density of 30,000 cells/well in the bottom of 24-well plates and the hydrogels were placed into the upper chamber with culture medium. After incubation for 1 and 3 days, the number of viable cells was determined qualitatively and quantitatively. (MAG = ×10). Each value represents the mean ± SD (n = 3). * denotes significant difference compared with 1 day of culture (p<0.05).

Figure 8 Dose effect of BMP-2 released from the CLF hydrogels on induction of alkaline phosphatase (ALP) activity in (a) W-20-17 and (b) C2C12 cells. Different

concentrations of BMP-2 (0, 50, 100, or 500 ng/ml) were loaded into the CLF hydrogels. The ALP activity was determined at 7 days of cultures and normalized for the dsDNA content. ALP activity is expressed as nmol/ng. Each value represents the mean ± SD (n = 3 per each group). * denotes significant difference compared with 7 days of culture of each group (p<0.05).

Figure 9 Dose effect of BMP-2 released from the CLF hydrogels on calcium mineral deposition in (a) W-20-17 and (b) C2C12 cells. Different concentrations of BMP-2 (0, 50, 100, or 500 ng/ml) were loaded into the CLF hydrogels. The presence of mineral within the cell layers was stained with Alizarin Red S (AR-S) staining solution at day 10 and 21. The red color areas and nodules demonstrate AR-S positive staining for calcium mineral in the cell layers (MAG = ×10).The calcium mineral contents were also quantitatively determined from Alizarin Red S staining extracts from the cell layers at day 10 and 21. Destained Alizarin Red S concentrations were determined at the absorbance of 405 nm and expressed as μg/ml. Each value represents the mean ± SD (n = 3 per each group). Each value represents the mean ± SD (n = 3). * denotes significant difference between groups at same time point (p<0.05). ** denotes significant difference in the same group at different time point (p<0.05).

Figure 10 Representative radiographs of the bone defects with implantation of CLF hydrogels containing different concentrations of BMP-2 (0, 0.5, 1, 2, or 5μg) taken at 2 and 4 weeks.

Figure 11 (a) Representative micro-computed tomography images of the bone defects implanted with CLF hydrogel containing different concentrations of BMP-2 (0, 0.5, 1, 2, or 5μg) at 4 weeks. (b) Quantification of regenerated bone volume within the bone defects. * denotes significant difference compared to the control CLF hydrogel groups with 0 μg BMP-2 (p<0.05).

Figure 12 Representative histological sections of the rat critical size femoral defects treated with CLF hydrogels containing different concentrations of BMP-2 (0, 0.5, 1, 2, or 5μg). The histological cross-sections were taken from the bone defect 4 weeks after surgery and stained with hematoxylin and eosin (H&E). (a) Representative low (×10) and (b) high magnification (×200) views of H&E show the extent of cellular infiltration and bone formation. The approximate boundary of the defect was denoted by the dashed lines. High magnification view was denoted by the red box. H, hydrogel; HB, host bone; NB, new bone; BM, bone marrow; O, osteoclasts; Ob, osteoblasts; Oc, osteocytes; BV, blood vessel.

Figure 1a

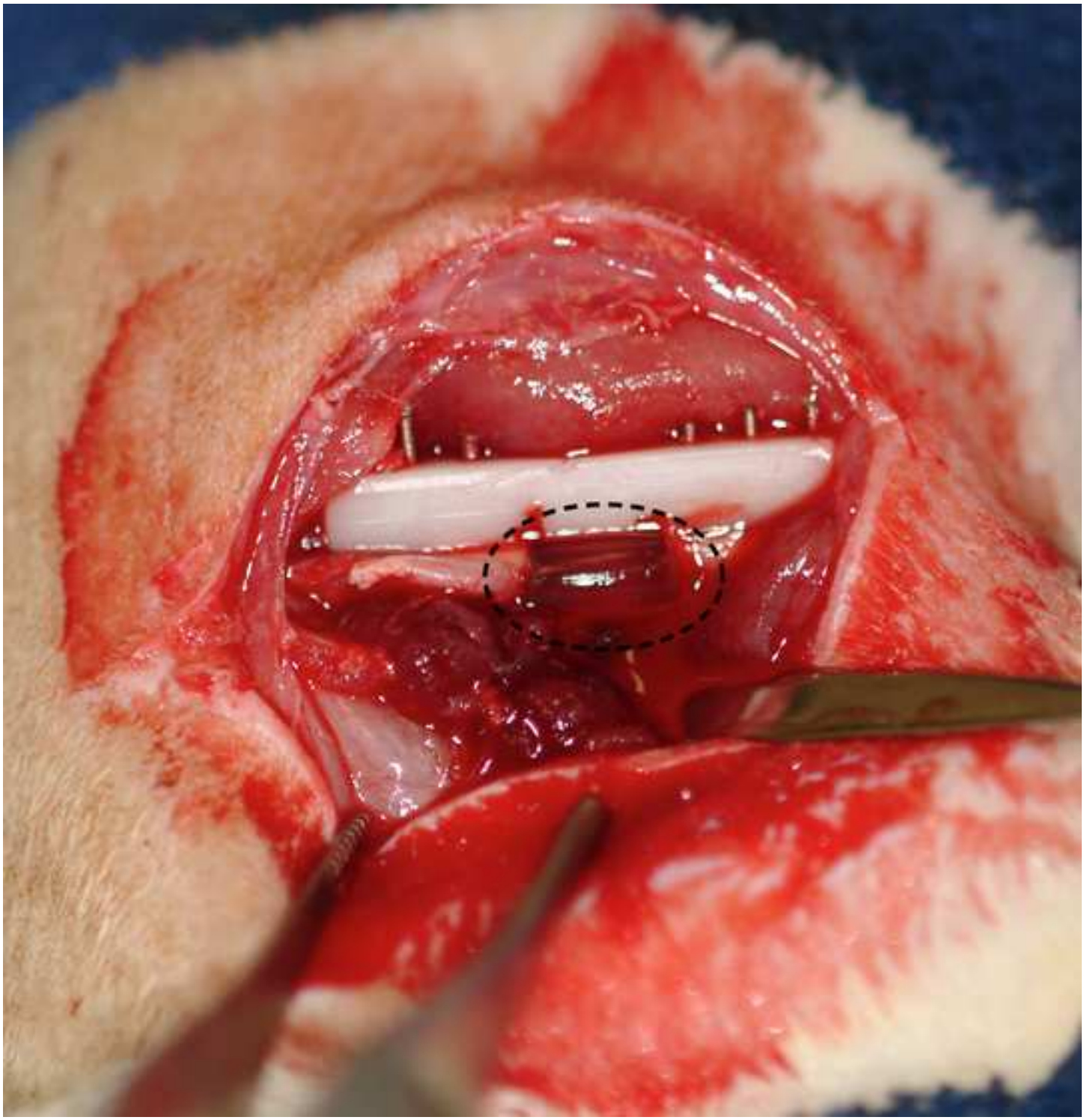

Figure 1b

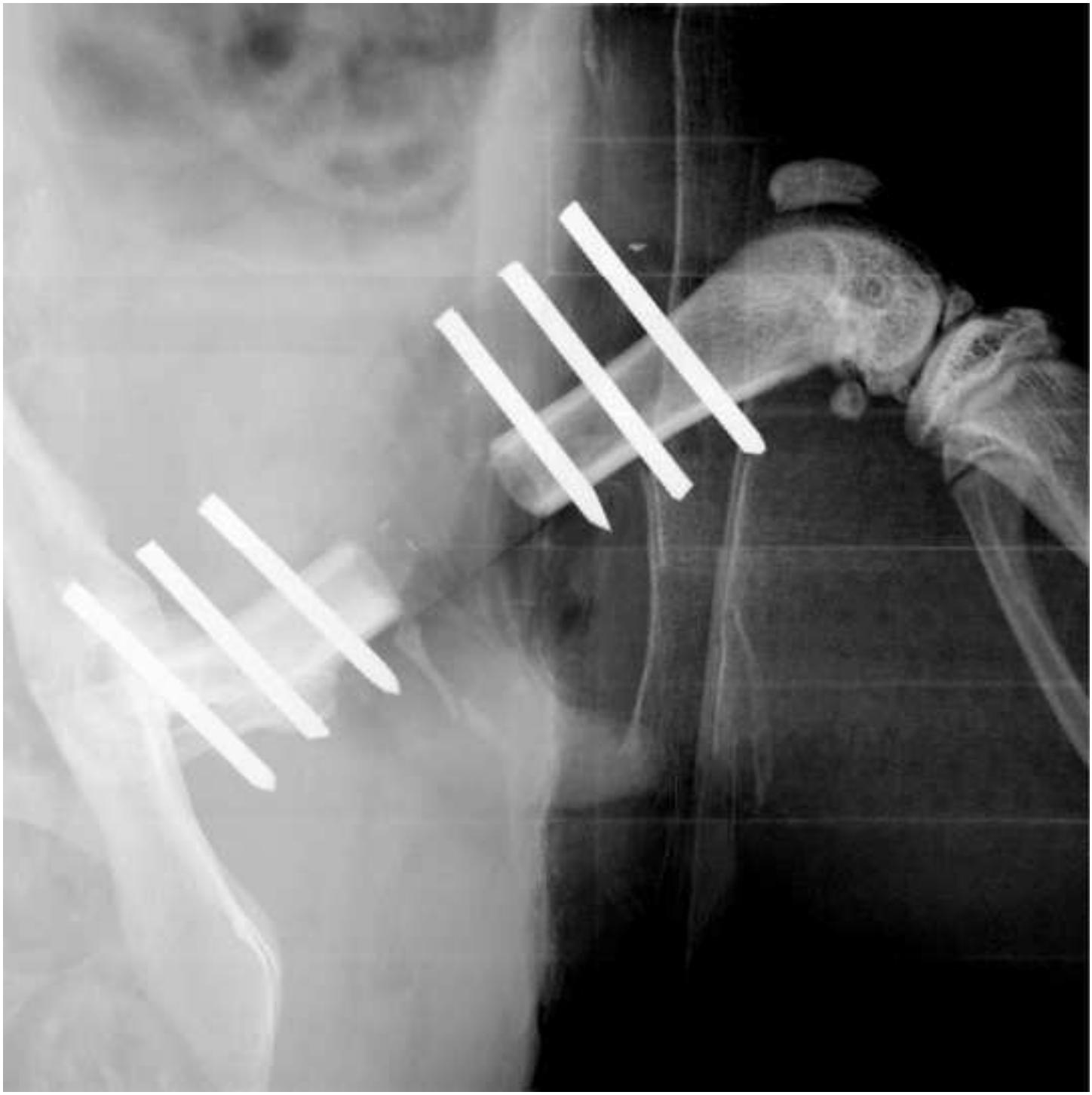

Figure 2

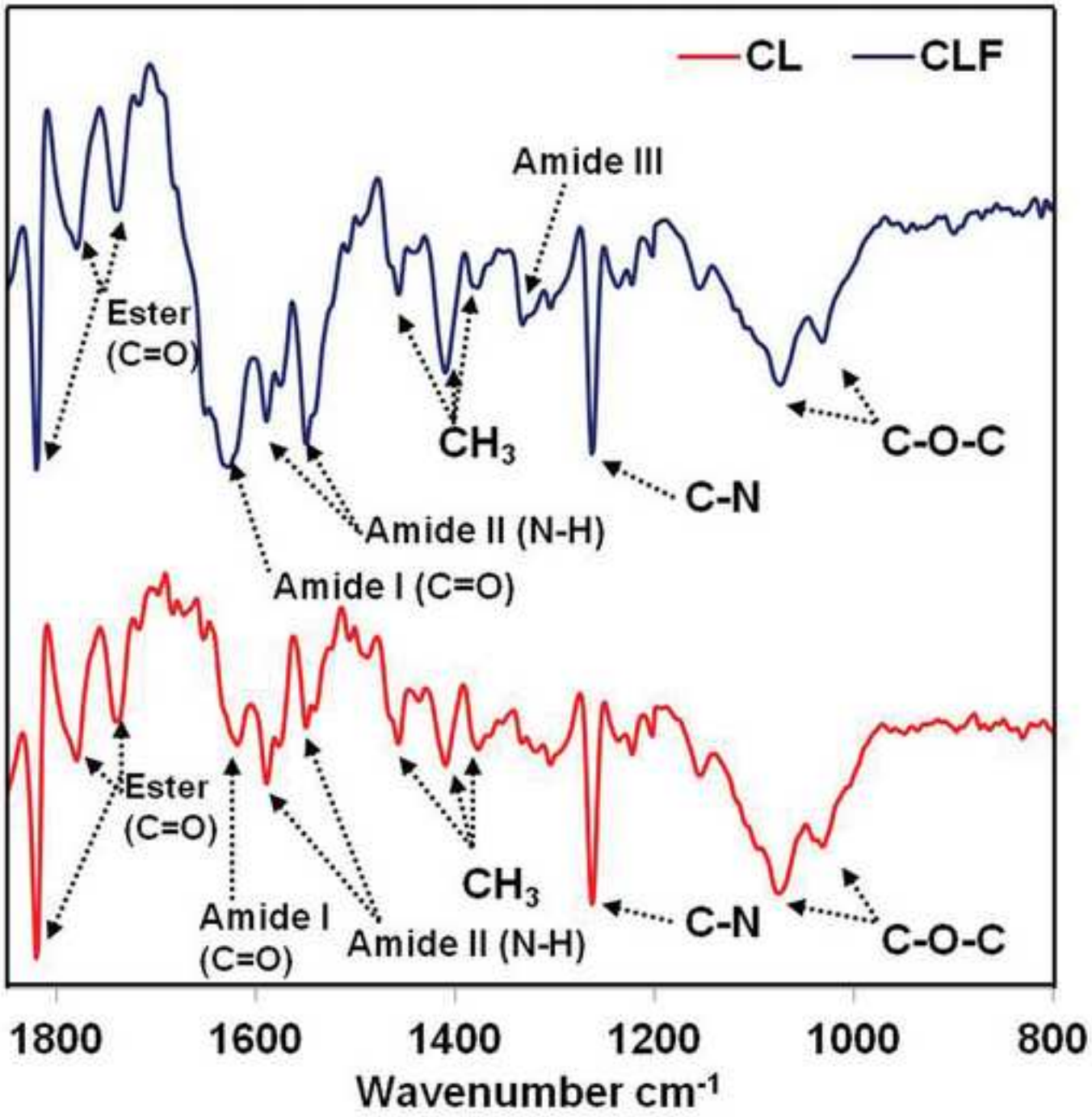

Figure 3

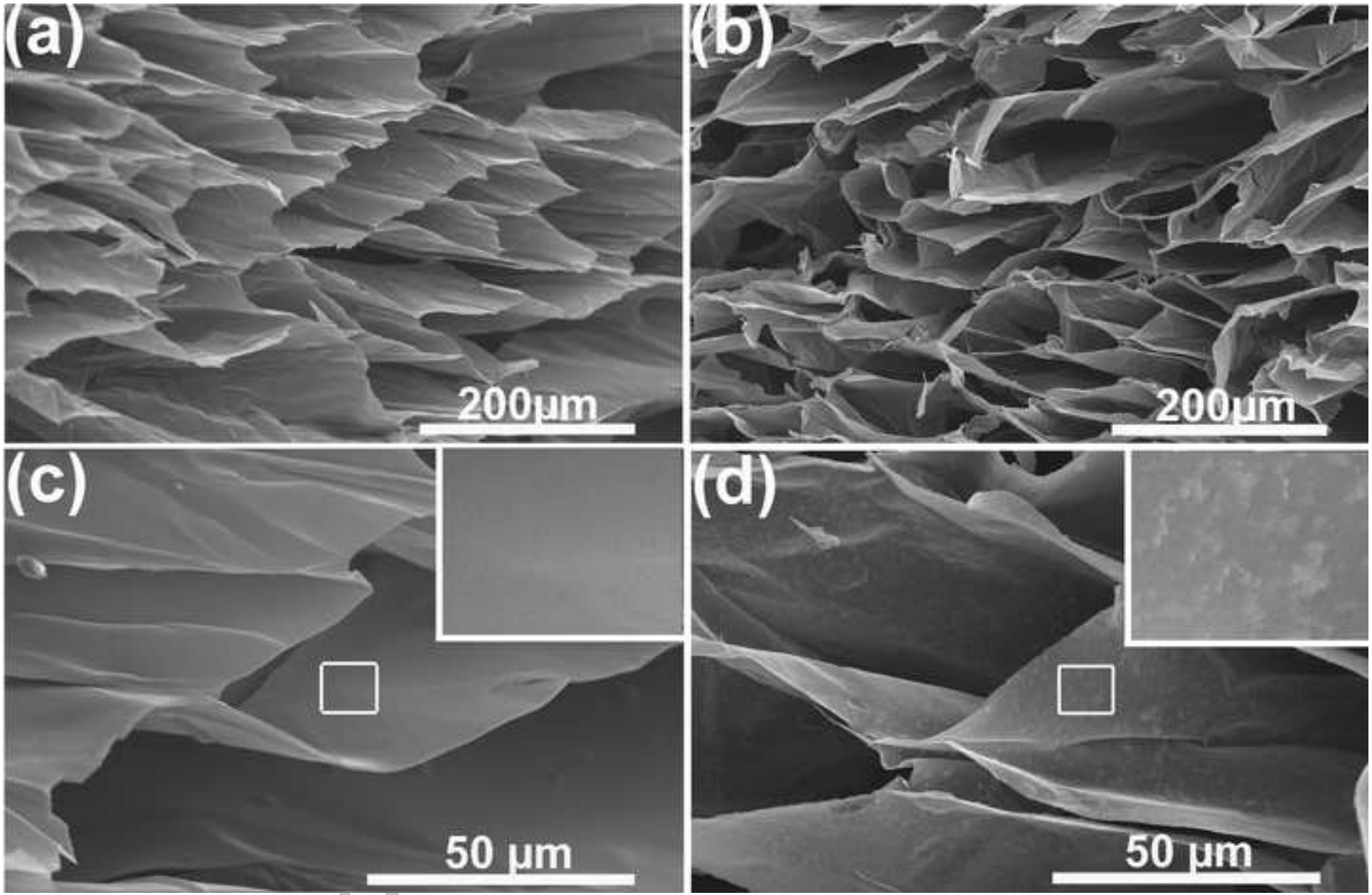

Figure 4a

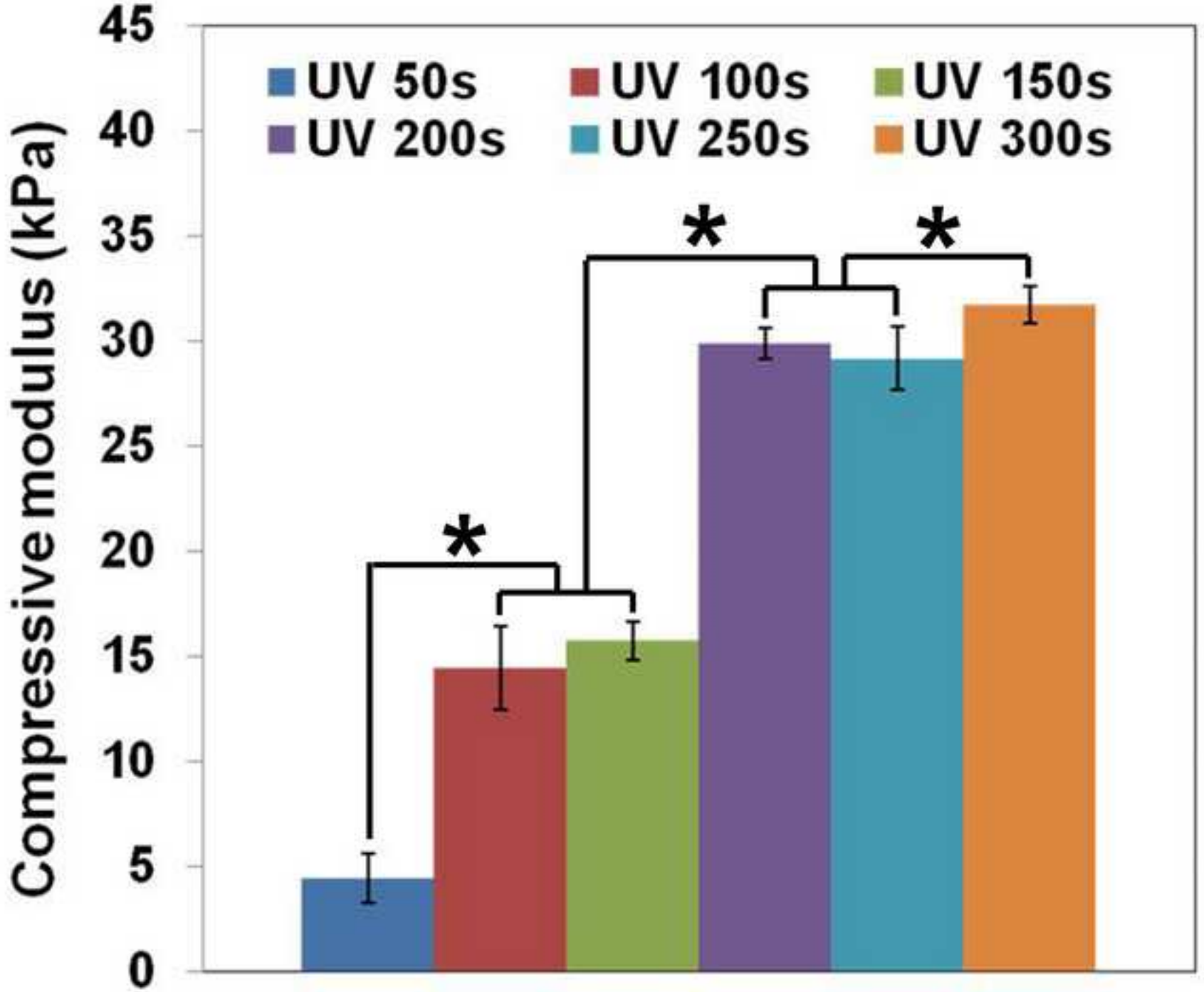

Figure 4b

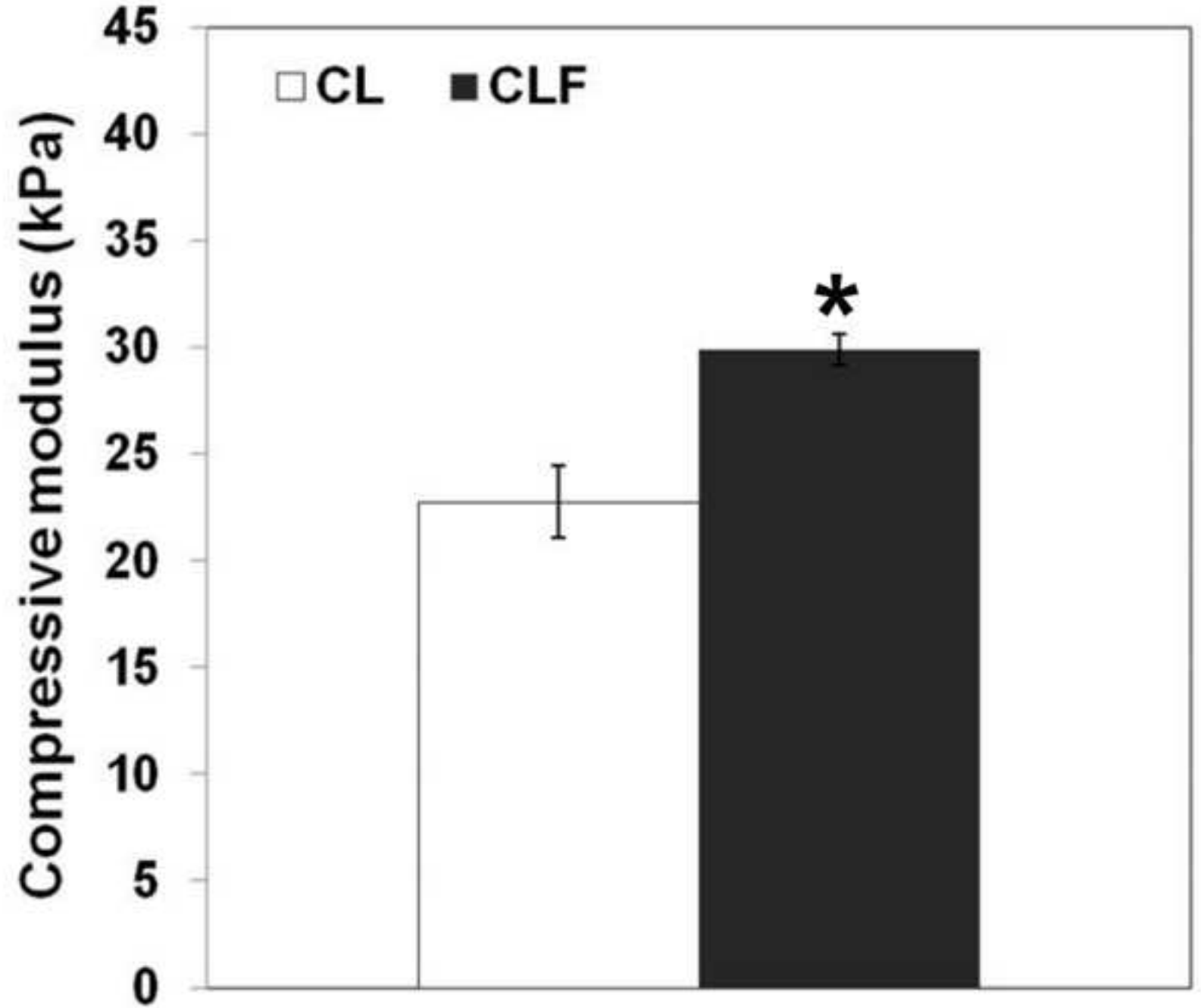

Figure 5a

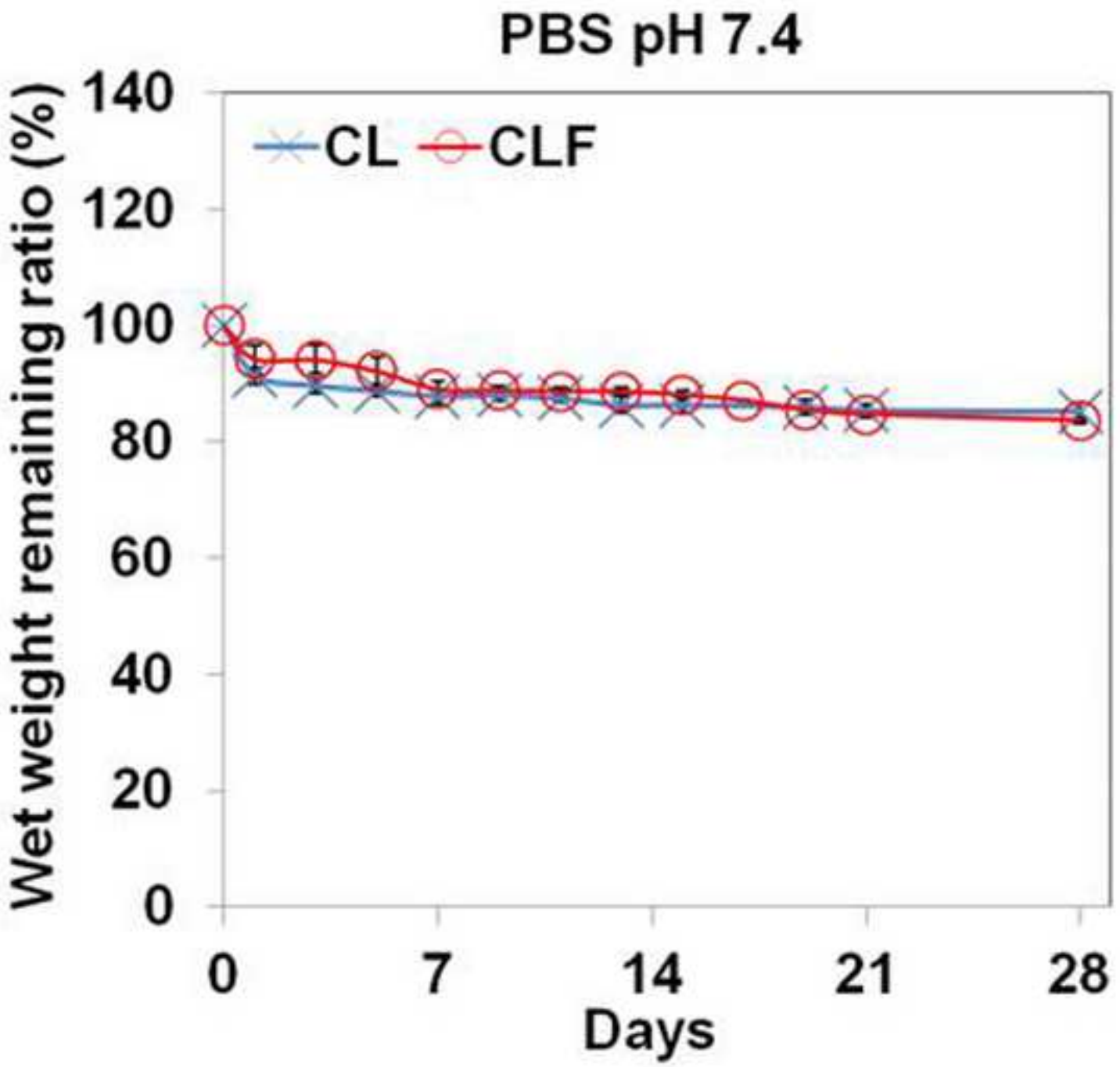

Figure 5b

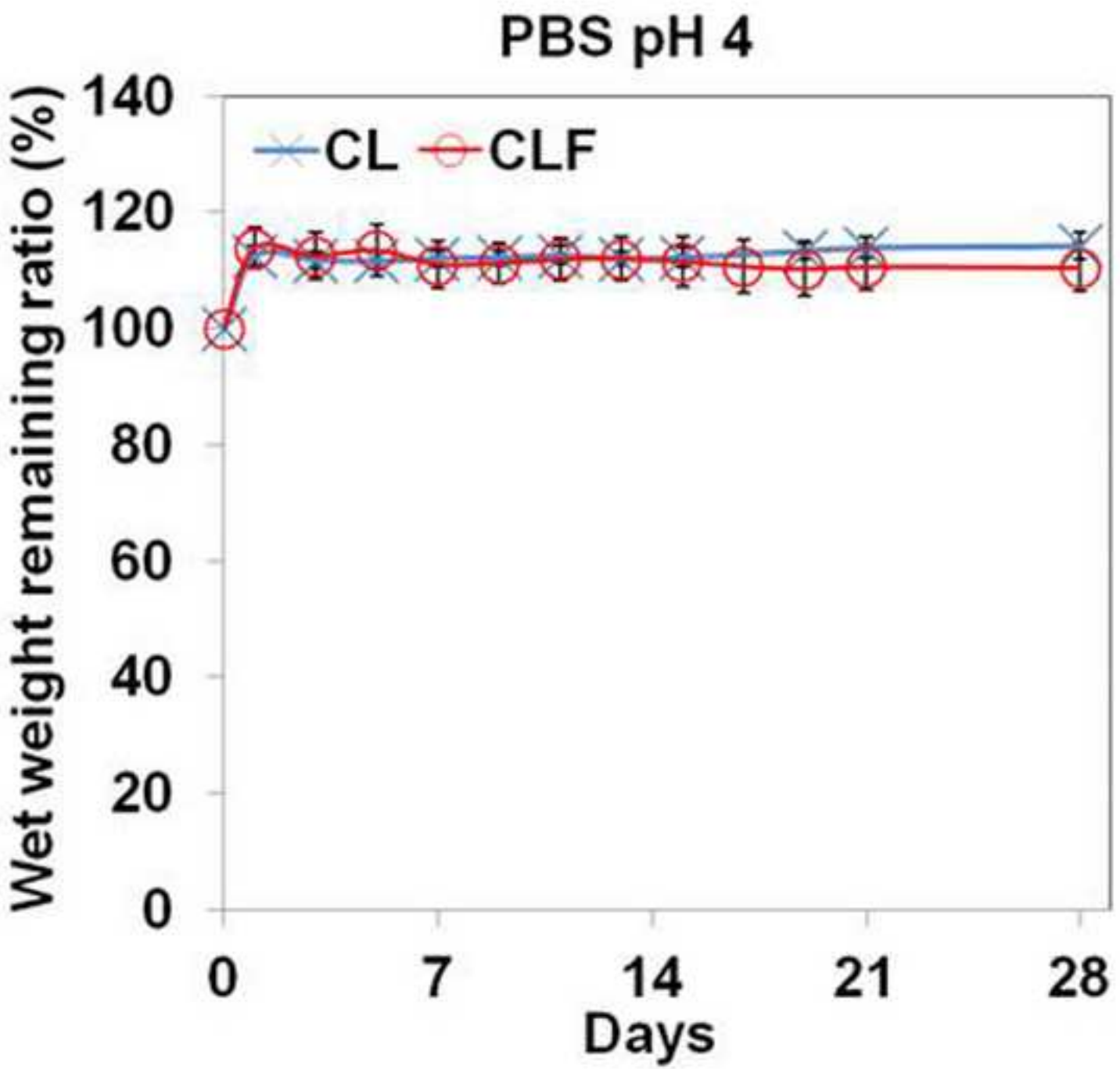

Figure 5c

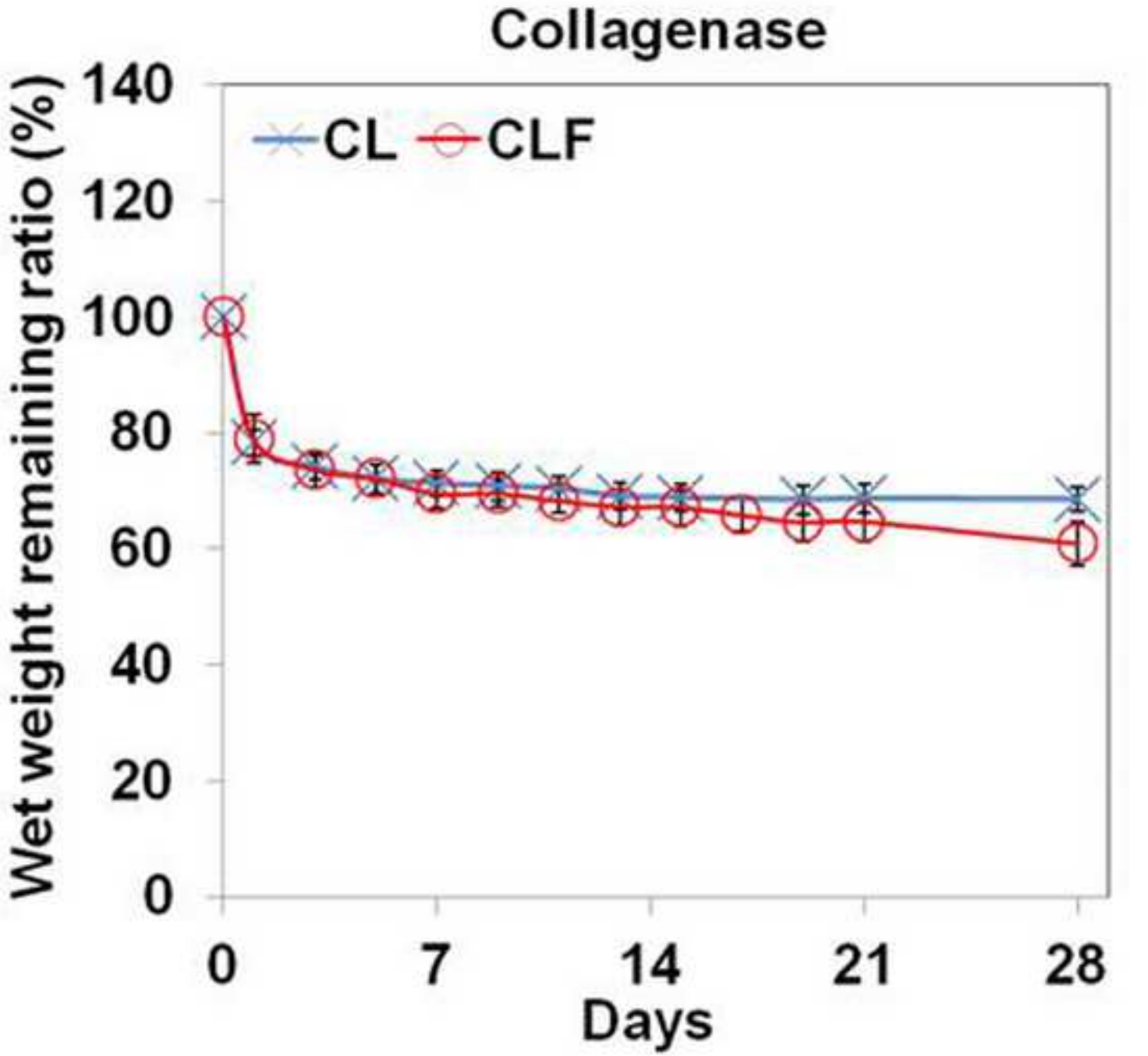

Figure 6a

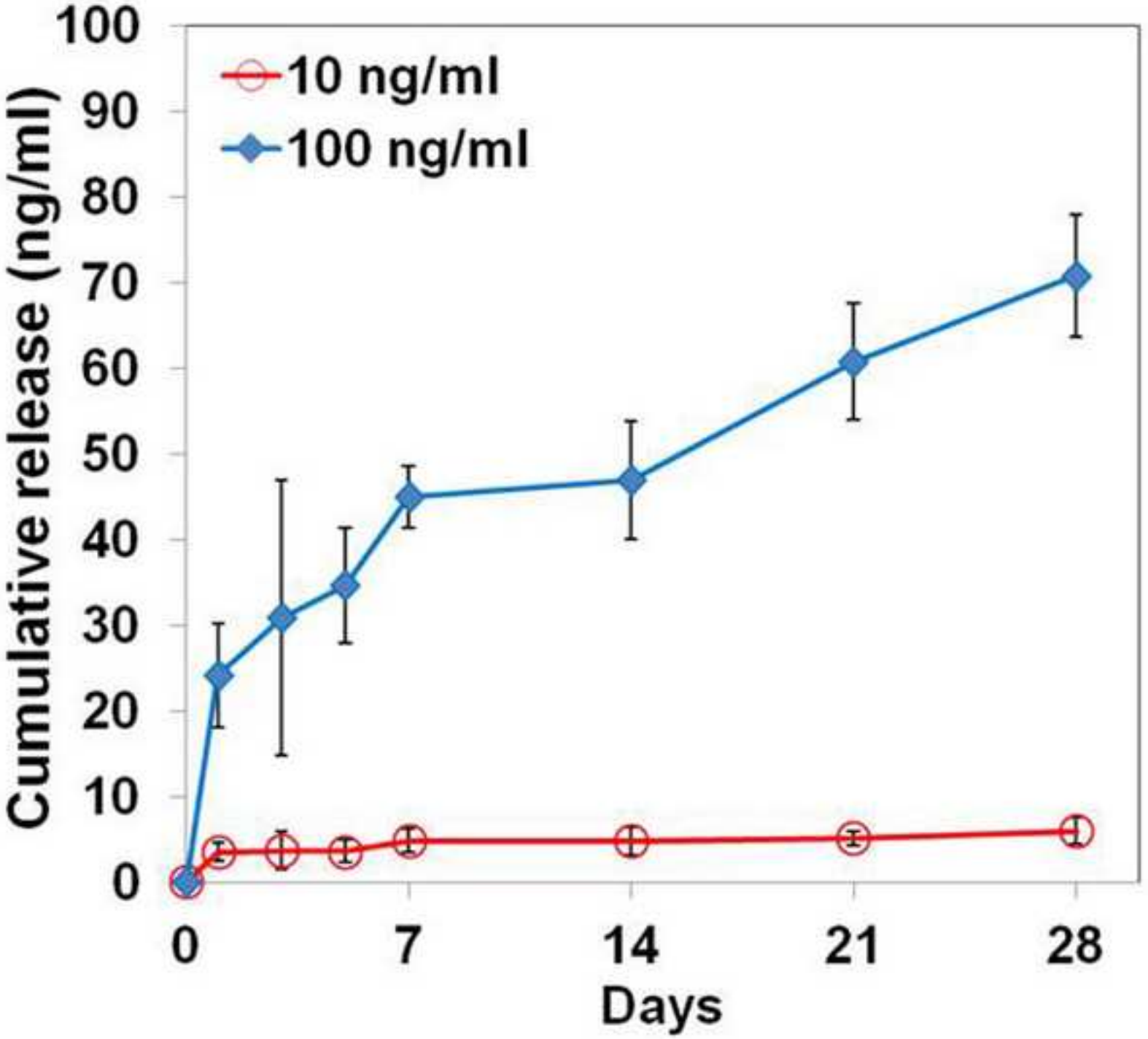

Figure 6b

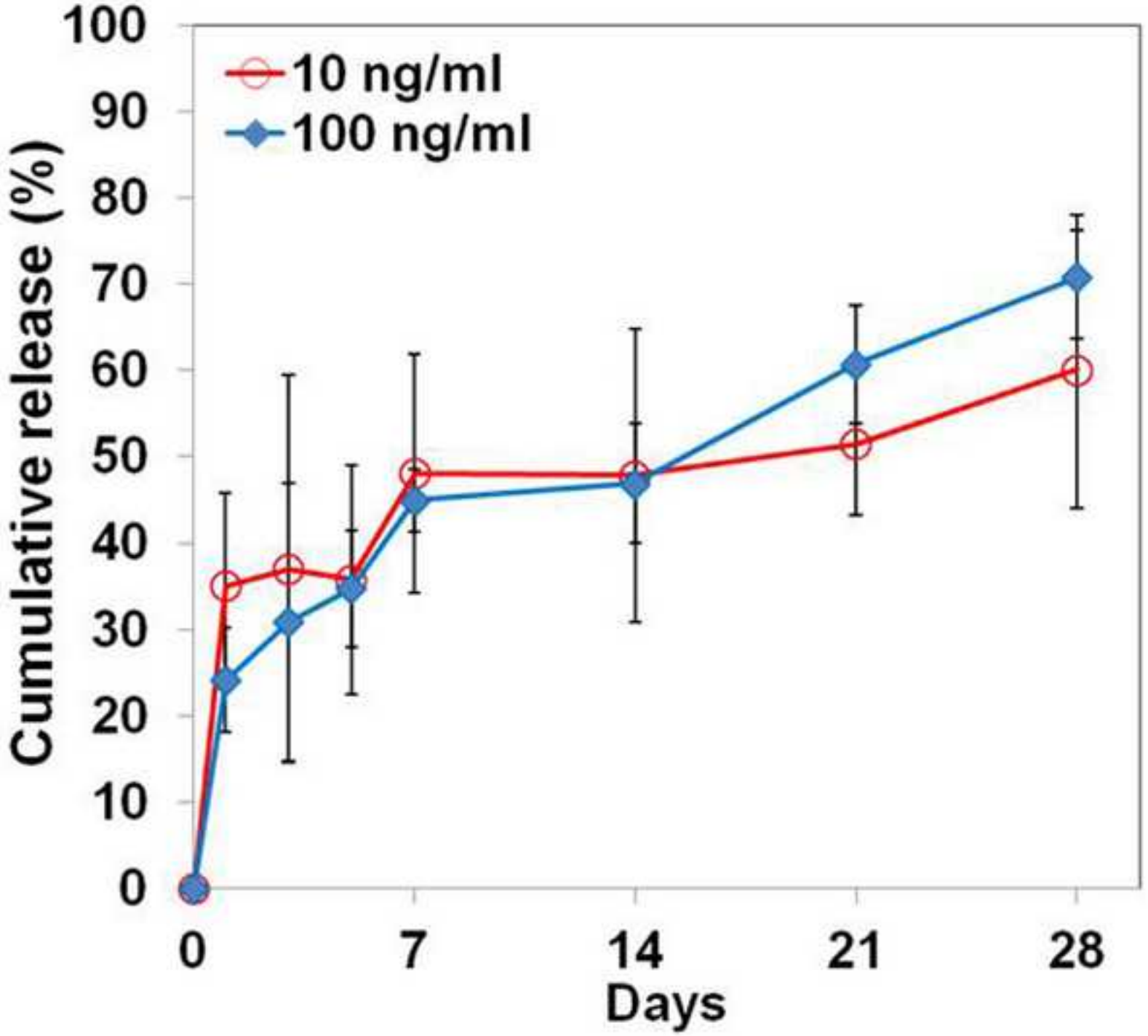

Figure 7a

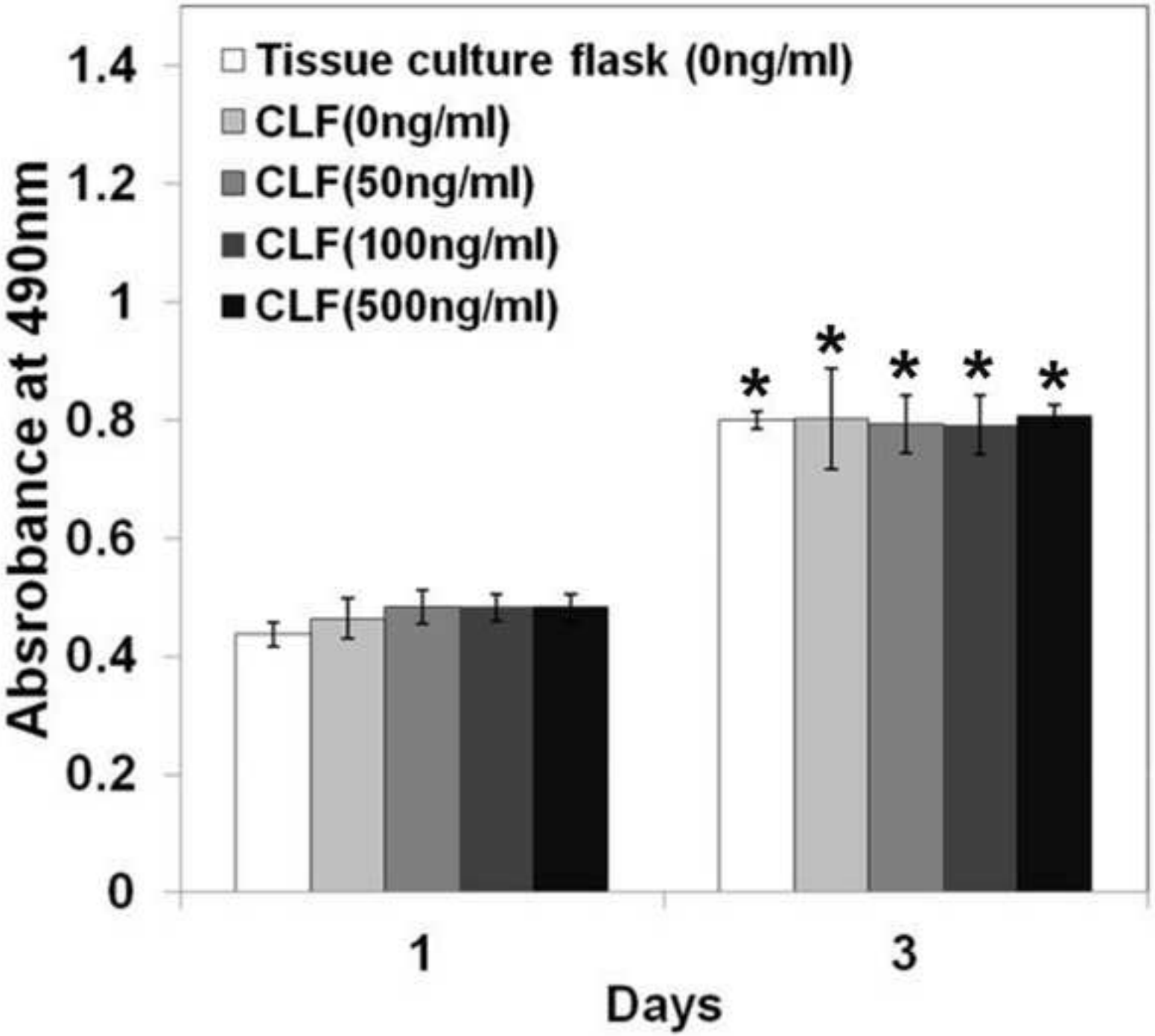

Figure 7b

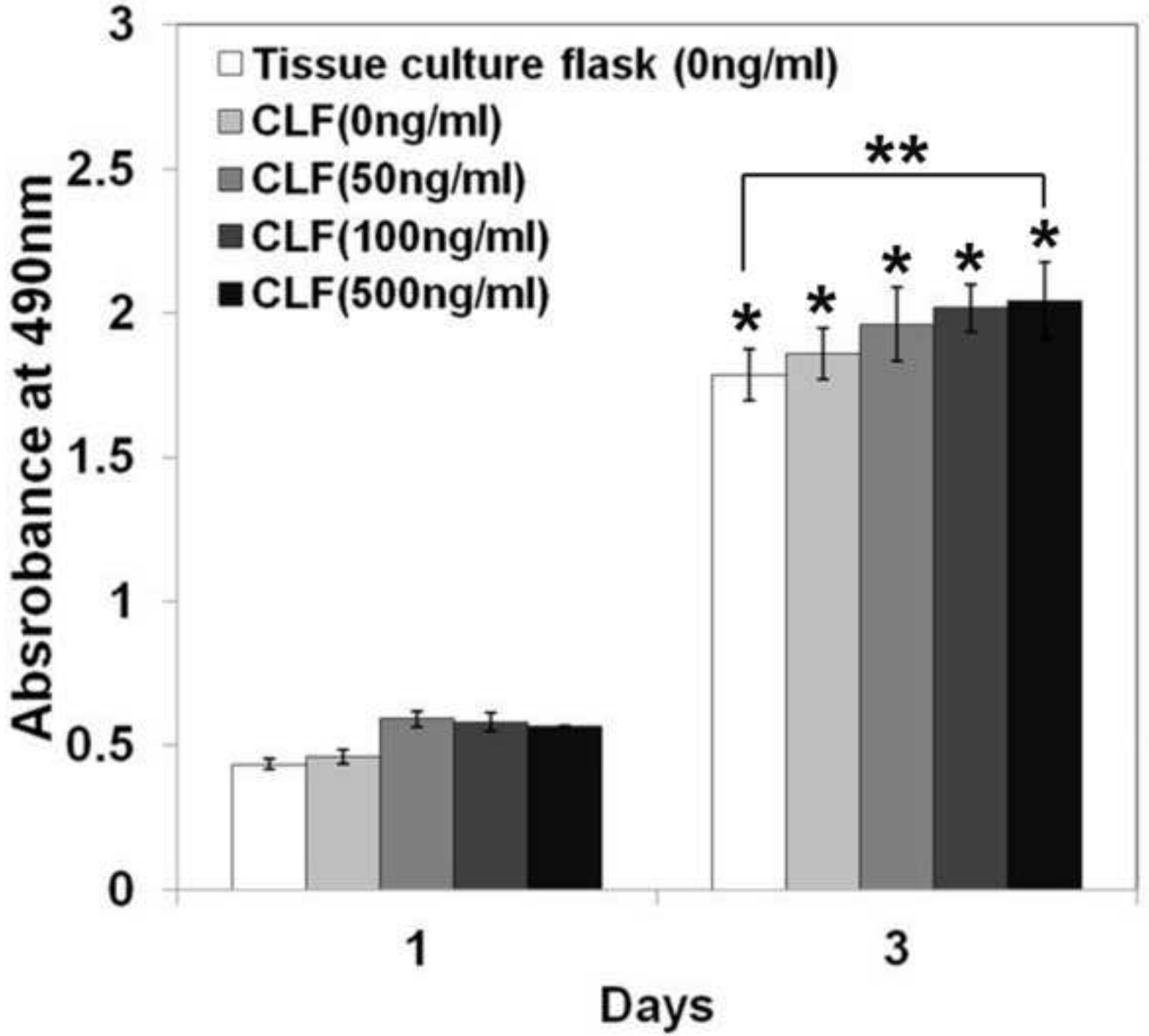

Figure 7c

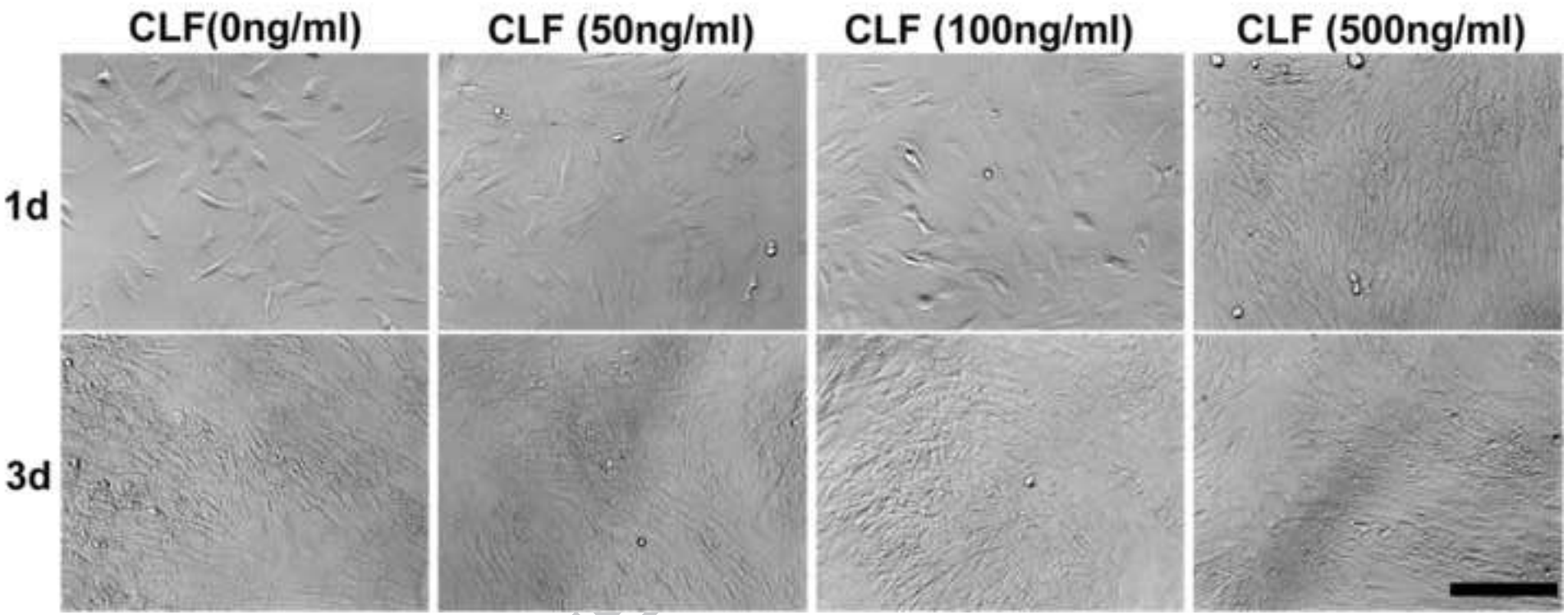

Figure 7d

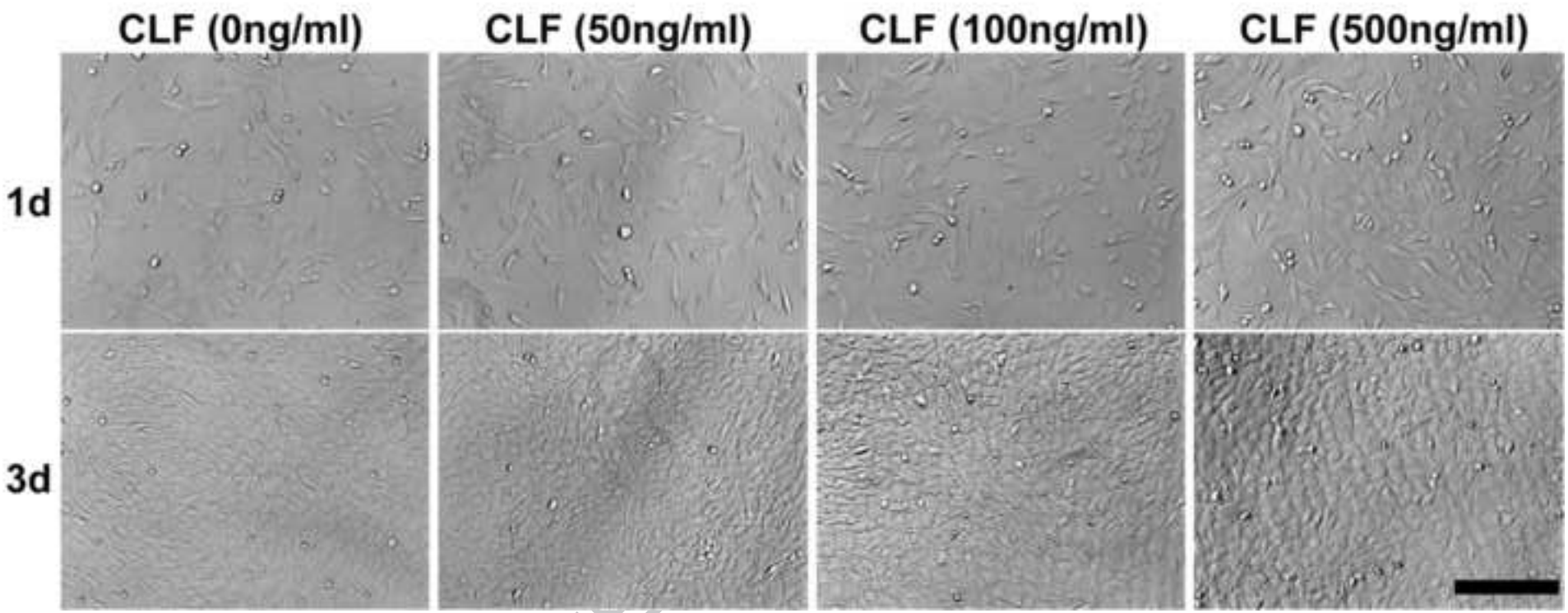

Figure 8a

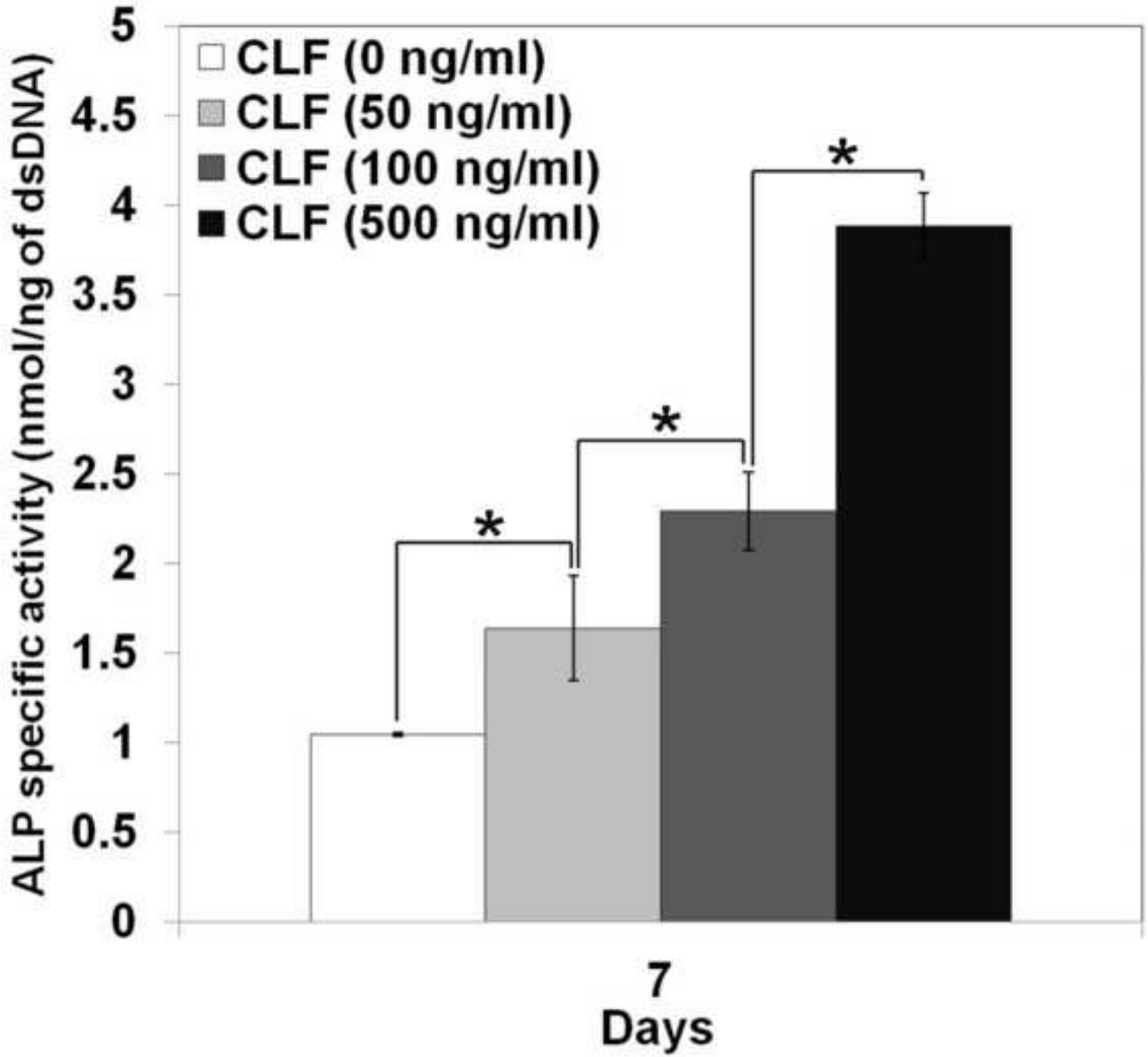

Figure 8b

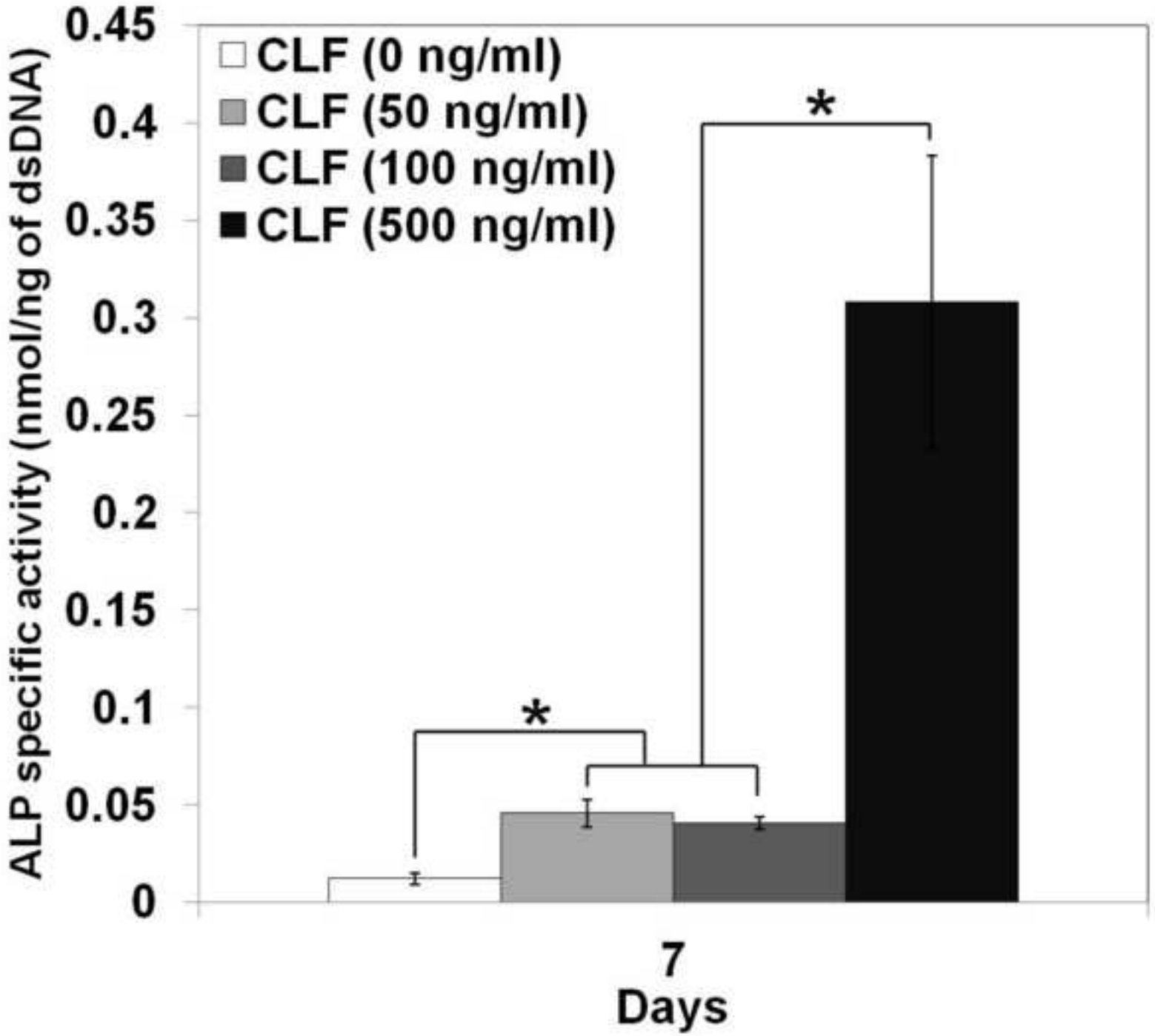

Figure 9a

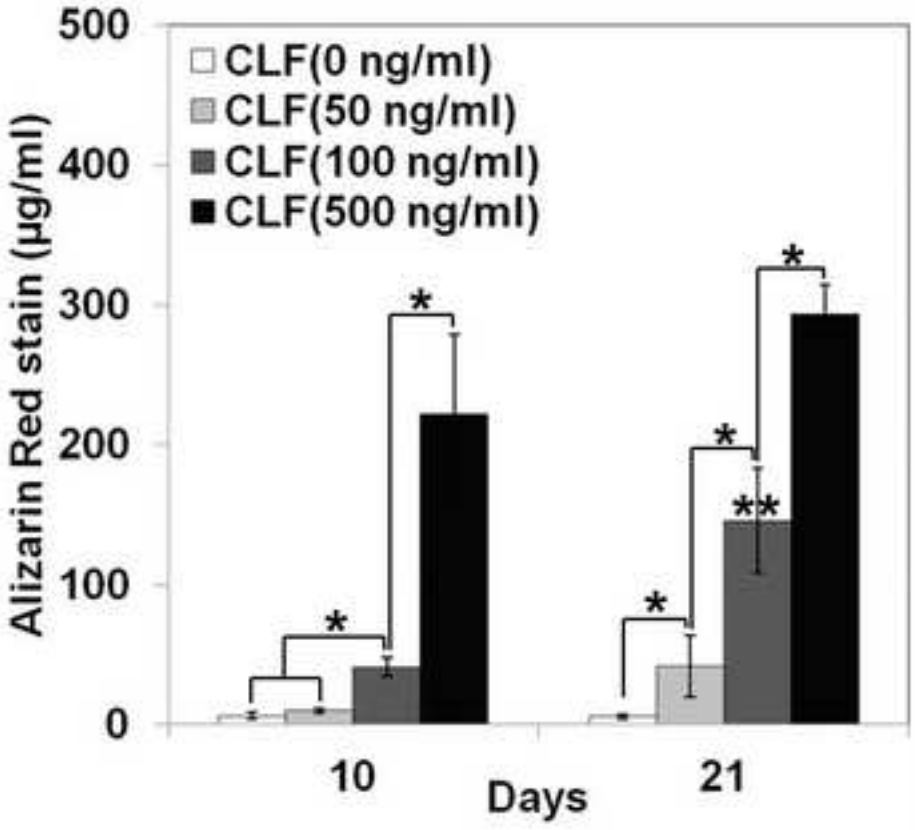

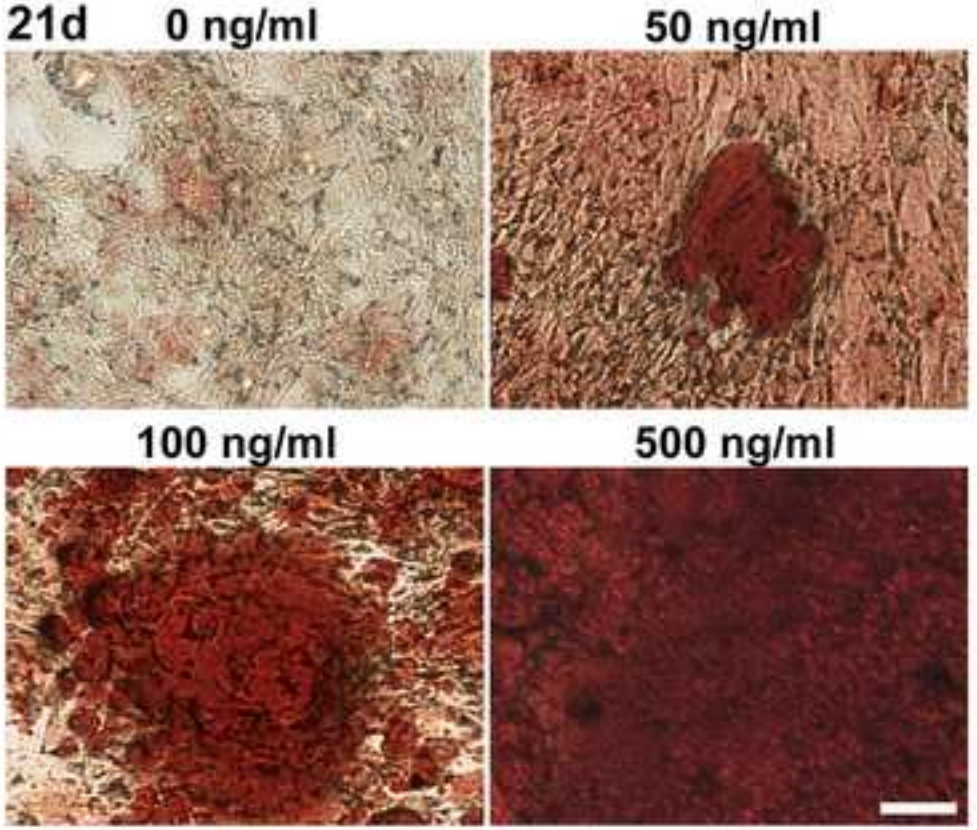

Figure 9b

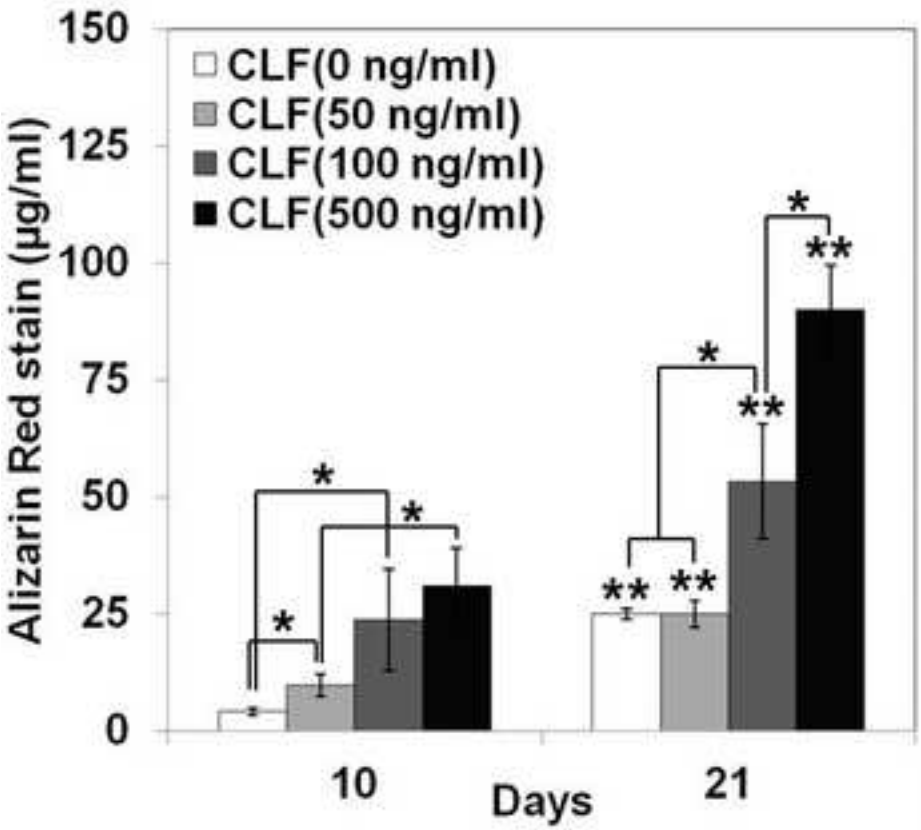

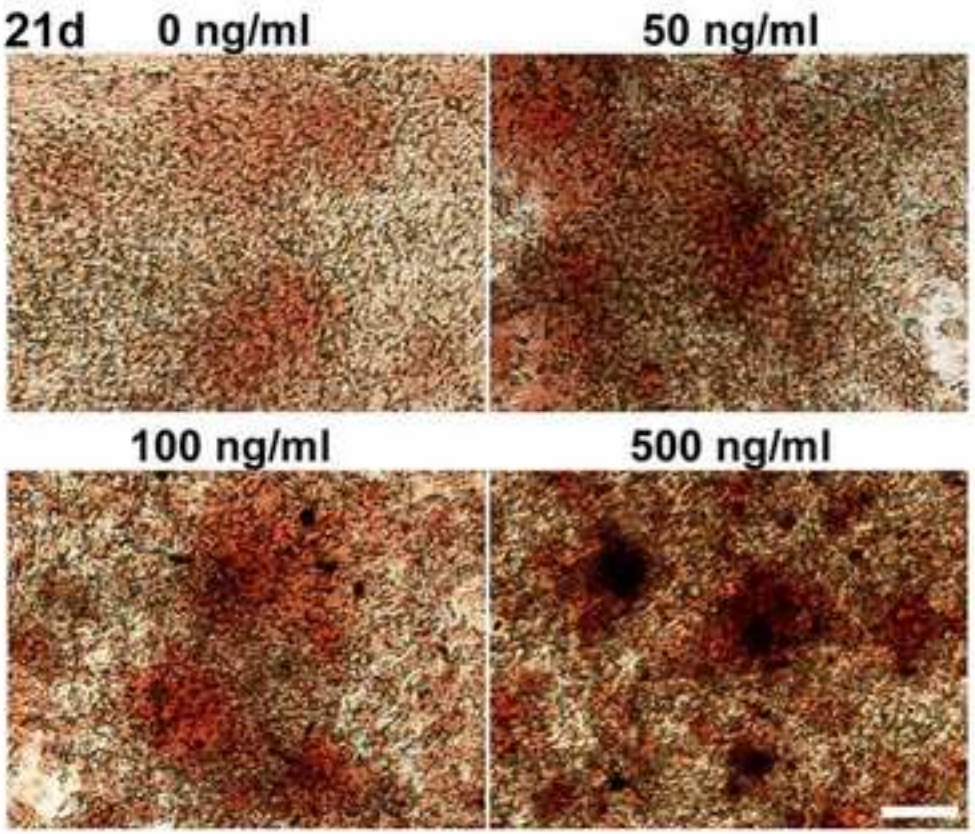

Figure 10

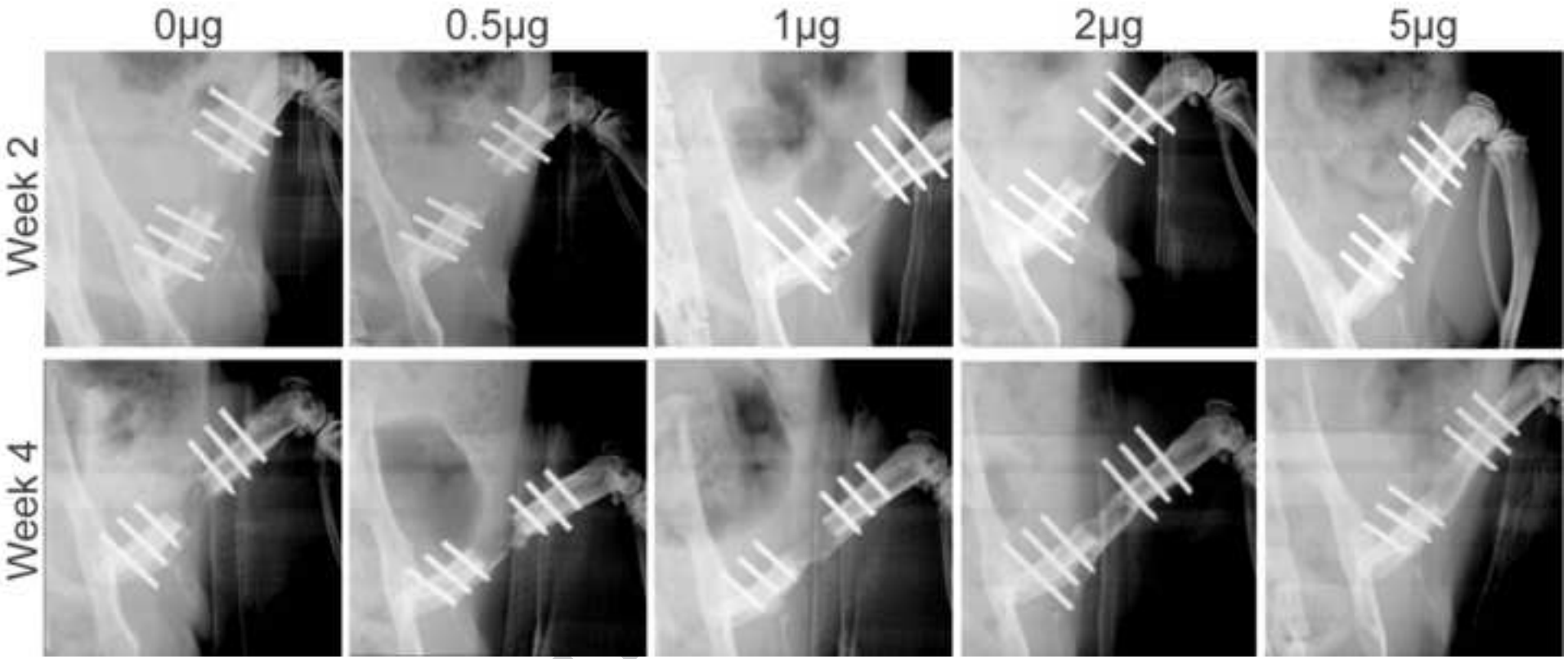

Figure 11a

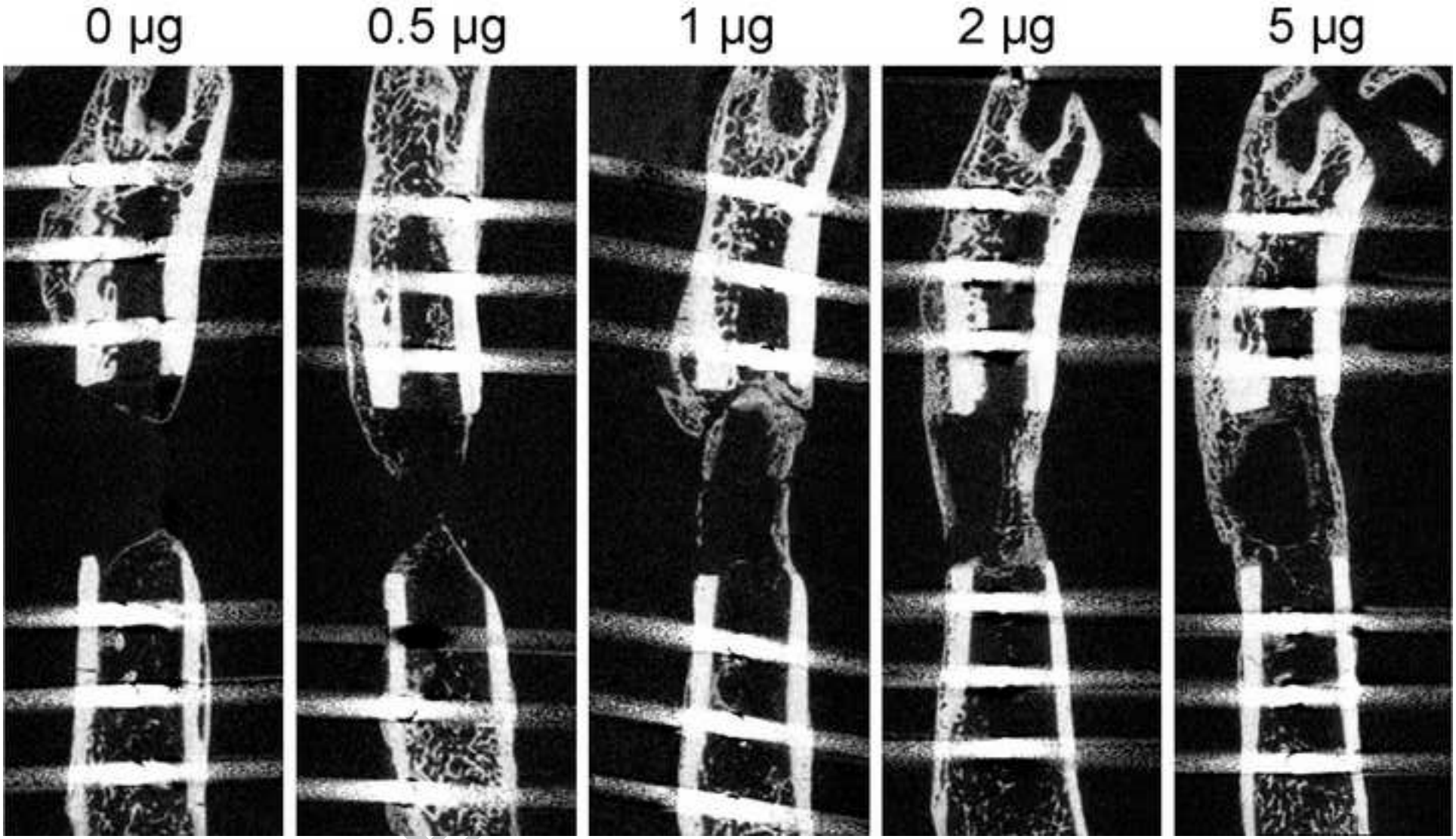

Figure 11b

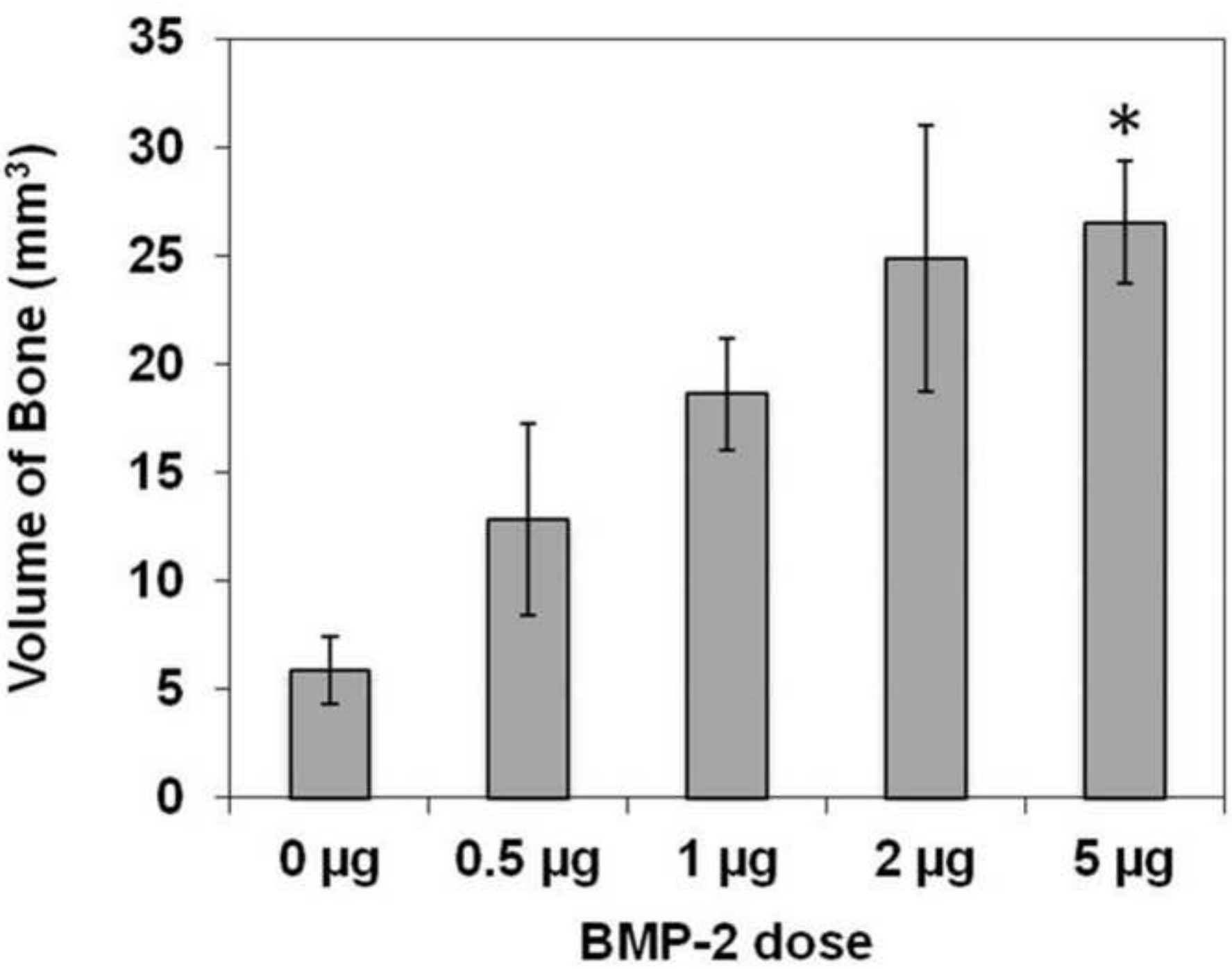

Figure 12

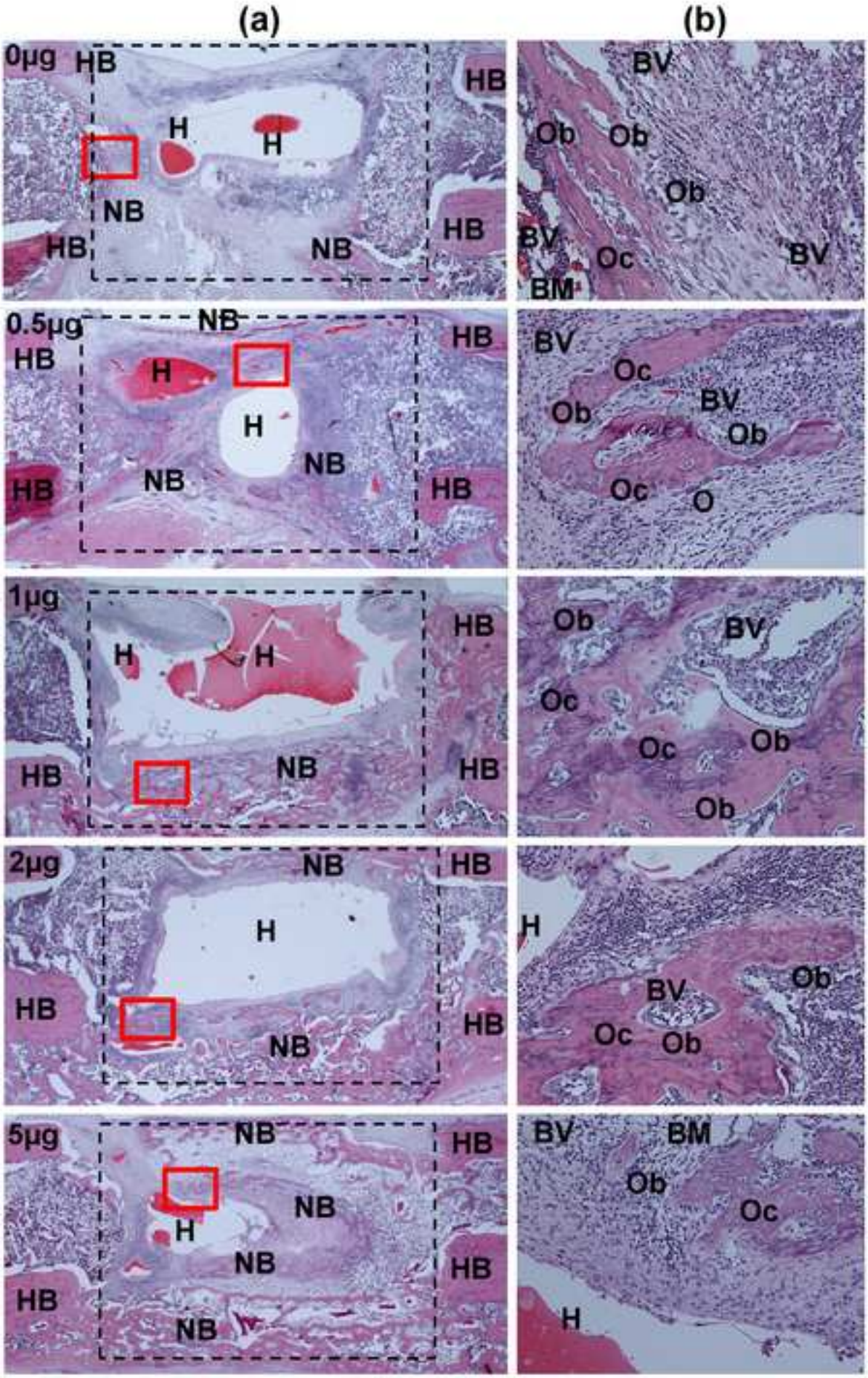

Graphical abstract